NASA/TP—2001–211302

Polymer Matrix Composite Lines and Ducts

(National Research Announcement 8–21 Final Report)

A.T. Nettles
Marshall Space Flight Center, Marshall Space Flight Center, Alabama

October 2001

The NASA STI Program Office…in Profile

Since its founding, NASA has been dedicated to the advancement of aeronautics and space science. The NASA Scientific and Technical Information (STI) Program Office plays a key part in helping NASA maintain this important role.

The NASA STI Program Office is operated by Langley Research Center, the lead center for NASA's scientific and technical information. The NASA STI Program Office provides access to the NASA STI Database, the largest collection of aeronautical and space science STI in the world. The Program Office is also NASA's institutional mechanism for disseminating the results of its research and development activities. These results are published by NASA in the NASA STI Report Series, which includes the following report types:

- TECHNICAL PUBLICATION. Reports of completed research or a major significant phase of research that present the results of NASA programs and include extensive data or theoretical analysis. Includes compilations of significant scientific and technical data and information deemed to be of continuing reference value. NASA's counterpart of peer-reviewed formal professional papers but has less stringent limitations on manuscript length and extent of graphic presentations.

- TECHNICAL MEMORANDUM. Scientific and technical findings that are preliminary or of specialized interest, e.g., quick release reports, working papers, and bibliographies that contain minimal annotation. Does not contain extensive analysis.

- CONTRACTOR REPORT. Scientific and technical findings by NASA-sponsored contractors and grantees.

- CONFERENCE PUBLICATION. Collected papers from scientific and technical conferences, symposia, seminars, or other meetings sponsored or cosponsored by NASA.

- SPECIAL PUBLICATION. Scientific, technical, or historical information from NASA programs, projects, and mission, often concerned with subjects having substantial public interest.

- TECHNICAL TRANSLATION. English-language translations of foreign scientific and technical material pertinent to NASA's mission.

Specialized services that complement the STI Program Office's diverse offerings include creating custom thesauri, building customized databases, organizing and publishing research results…even providing videos.

For more information about the NASA STI Program Office, see the following:

- Access the NASA STI Program Home Page at ***http://www.sti.nasa.gov***

- E-mail your question via the Internet to help@sti.nasa.gov

- Fax your question to the NASA Access Help Desk at (301) 621–0134

- Telephone the NASA Access Help Desk at (301) 621–0390

- Write to:
  NASA Access Help Desk
  NASA Center for AeroSpace Information
  7121 Standard Drive
  Hanover, MD 21076–1320

NASA/TP—2001–211302

Polymer Matrix Composite Lines and Ducts

(National Research Announcement 8–21 Final Report)

A.T. Nettles
Marshall Space Flight Center, Marshall Space Flight Center, Alabama

National Aeronautics and
Space Administration

Marshall Space Flight Center • MSFC, Alabama 35812

October 2001

TRADEMARKS

Trade names and trademarks are used in this report for identification only. This usage does not constitute an official endorsement, either express or implied, by the National Aeronautics and Space Administration.

Available from:

NASA Center for AeroSpace Information
7121 Standard Drive
Hanover, MD 21076–1320
(301) 621–0390

National Technical Information Service
5285 Port Royal Road
Springfield, VA 22161
(703) 487–4650

TABLE OF CONTENTS

1. INTRODUCTION 1

2. TEST ARTICLE 3

2.1 Conventional Hand Layup 4
2.2 Solvent-Assisted Resin Transfer Molding 6
2.3 Thermoplastic Tape Laying 7

3. TESTING 10

3.1 Nondestructive Evaluation Testing 10
3.2 Proof Testing 11
3.3 Leak Testing 12
3.4 Cryogenic Testing 12
3.5 Burst Pressure Testing 14
3.6 Damage Tolerance 14

4. RESULTS 15

4.1 Nondestructive Evaluation Testing 15
4.2 Proof and Leak Testing 25
4.3 Cryogenic Testing 30
4.4 Burst Pressure Testing 33
4.5 Damage Tolerance Testing 35
4.6 Permeability After Impact Testing 50

5. ANALYSIS 64

6. DISCUSSION AND CONCLUSIONS 66

REFERENCES 67

LIST OF FIGURES

1. Drawing with dimensions of the common test article 3

2. Reusable tool used for HLU 4

3. Completed test article manufactured by HLU 5

4. View of flange area on a feedline manufactured via HLU 5

5. Microstructure of feedline manufactured via HLU:
(a) Longitudinal view and (b) radial view 6

6. Completed test article manufactured via SARTM 6

7. View of flange area of a feedline manufactured via SARTM 7

8. Microstructure of feedline manufactured via SARTM:
(a) Longitudinal view and (b) radial view 7

9. A test article being manufactured by TTL 8

10. Completed test article manufactured via TTL 8

11. View of flange area of a feedline manufactured via TTL 9

12. Microstructure of feedline manufactured via TTL:
(a) Longitudinal view and (b) radial view 9

13. Flash thermography image showing foreign object
(plastic tape) inclusion 10

14. Schematic showing placement of array of foil markers 11

15. Thermograph of position E12 on test article No. 3 11

16. Leak as detected by bubble-type solution in a test article 12

17. Location of 17 biaxial strain gauges on the test articles 14

18. Anomaly noted on thermograph of feedline HLU–2 15

LIST OF FIGURES (Continued)

19. Large inclusion found on feedline HLU–3 16

20. Cross section of plastic tape causing anomaly in figure 13 16

21. Dark regions and anomaly found in tube HLU–4 17

22a. No surface features, but strong thermal indication. Possible "thin film" inclusion 17

22b. No surface features. Unknown source 18

22c. No surface features but strong thermal indication. The blurred edges may indicate that this is a delamination from impact 18

22d. A bump is visible on the surface indicating an inclusion with possible internal void 19

22e. The surface of the tube shows signs of overworking during fabrication. These regions may be thin, resin-starved zones (indicated by the arrows) 19

22f. The surface of the tube has a small bump, which would indicate an inclusion 20

22g. Possible voids along a seam 20

23. Anomalies on feedline HLU–6 21

24. Thermography image of scuff on feedline HLU–7 21

25. Thermograph of possible deep inclusion on feedline HLU–7 22

26. Anomalies in feedline HLU–8 22

27. Thermograph showing thinning in feedline SARTM–2 23

28. Thermograph of thinning in feedline SARTM–3 24

29. Sample thermograms from feedline TTL–1 showing regions where the tape was not well consolidated in acreage and voids in flanges 24

LIST OF FIGURES (Continued)

30. Two areas of pinhole leaks on feedline HLU–5 26

31. Samples of leak areas on feedline HLU–6 26

32. Feedline SARTM–1 showing three leak paths 27

33. Feedline SARTM–3 showing one large leak path 28

34. Cross section of leak area on feedline SARTM–1 28

35. Cross section of leak area on feedline SARTM–3 29

36. Feedline TTL–2 showing ring of leakage around flange buildup area 29

37. Flange area of feedline TTL–3 showing gross leakage 30

38. Test article HLU–2 in test stand 300. Shown with full insulation and half of the insulation removed 31

39. Leakage across feedline SARTM–2 after first introduction of LN_2 into the feedline 32

40. Inside surface of SARTM feedlines: (a) No cryogenic temperature and (b) LN_2 temperature excursion 33

41. Outside surface of SARTM feedlines: (a) No cryogenic temperature and (b) LN_2 temperature excursion 33

42. Feedline HLU–2 after failing at 545-psi internal pressure 34

43. Feedline HLU–7 after failing at 364-psi internal pressure 34

44. Typical damage to impacted side of specimens at 2.5 ft-lb 38

45. Typical damage to nonimpacted side of specimens at 2.5 ft-lb 39

46. X rays of specimens impacted at 2.5 ft-lb 40

47. Cross-sectional photomicrographs of specimens impacted at 2.5 ft-lb 41

48. Cross-sectional photomicrographs of specimens impacted at 2.5 ft-lb, fluorescent dye enhanced 43

LIST OF FIGURES (Continued)

49. Typical damage to impacted side of specimens at 1.8 ft-lb 45

50. Typical damage to nonimpacted side of specimens at 1.8 ft-lb 47

51. Cross-sectional photomicrographs of specimens impacted at 1.8 ft-lb 48

52. Schematic of impact apparatus 51

53. Schematic of leak detection apparatus 52

54. Specimen displaying a leak using a bubble-type leak detection fluid 52

55. Surface views of impacted HLU specimens 53

56. Leak check images of HLU specimens 55

57. Flow rate (permeability) versus applied pressure for specimen 3A 57

58. Flow rate (permeability) versus applied pressure for specimen 3B 57

59. Flow rate (permeability) versus applied pressure for specimen 4A 58

60. Flow rate (permeability) versus applied pressure for specimen 4B 58

61. Flow rate (permeability) versus applied pressure for specimen 5A 59

62. Flow rate (permeability) versus applied pressure for specimen 5B 59

63. Flow rate (permeability) versus applied pressure for specimen 6B 60

64. Surface views of electron beam-impacted specimens 61

65. Examples of large areas of leakage on electron beam-cured laminates 62

LIST OF TABLES

1. Cryogenic testing series 12

2. Materials tested for impact resistance 36

3. Predicted and actual hoop strain data for feedline HLU #2 64

4. Predicted and actual hoop strain data for feedline HLU #7 65

LIST OF ACRONYMS

GHe	gaseous helium
GN_2	gaseous nitrogen
GRC	Glenn Research Center
He	helium
HLU	hand layup
LH_2	liquid hydrogen
LN_2	liquid nitrogen
MSFC	Marshall Space Flight Center
NDE	nondestructive evaluation
ORNL	Oak Ridge National Laboratories
PEC	Productivity Enhancement Center
PEEK	polyetheretherketone
PMC	polymer matrix composite
SARTM	solvent assisted resin transfer molding
TP	Technical Publication
TTL	thermoplastic tape laying
UV	ultraviolet
ZnI_2	zinc iodide

TECHNICAL PUBLICATION

POLYMER MATRIX COMPOSITE LINES AND DUCTS

(National Research Announcement 8–21 Final Report)

1. INTRODUCTION

The Access-to-Space study identified the requirement for lightweight structures to achieve orbit with a single-stage vehicle.[1] The use of composite components is critical to fulfilling that requirement. The purpose of this task is to extend previous efforts with polymer matrix composite (PMC) feedlines and ducts.

This Technical Publication (TP) outlines the results of a task that was awarded under National Research Announcement 8–21. This task is an element under the Reusable Launch Vehicle Focused Technology Project Plan. The task is titled "Polymer Matrix Composite (PMC) Lines and Ducts" and its main objective was to demonstrate the feasibility of manufacturing a large diameter composite feedline with a 90° elbow section and integral flanges. Other objectives of the task were to demonstrate PMC performance under cryogenic environments, to demonstrate knowledge of the damage tolerance issues associated with composite feedlines, and to evaluate feedlines manufactured by four different techniques. To accomplish these objectives, an 8-in.-diameter composite feedline for liquid hydrogen (LH_2) service was selected to be designed because it is typical of those found in a launch vehicle main propulsion system.

While most feedline concepts currently use a metallic material, a small composite feedline was successfully used on the Delta Clipper–Experimental Advanced flight vehicle. Larger feedlines of more complexity need to be developed to realize even larger savings in weight. Typically, a composite feedline can save over 50 percent mass to be manufactured via four different technologies: (1) Conventional hand layup (HLU) and autoclave cure, (2) solvent-assisted resin transfer molding (SARTM), (3) electron beam cure, and (4) thermoplastic tape laying (TTL).

NASA Marshall Space Flight Center (MSFC) was responsible for material selection and manufacture of the feedlines made via the HLU method. NASA Glenn Research Center (GRC) was responsible for material selection and manufacture of feedlines made by the SARTM process. Oak Ridge National Laboratories (ORNL) was responsible for material selection and manufacture of feedlines to be made by the electron beam cure process. Automated Dynamics Incorporated manufactured feedlines by TTL.

The inspection, analysis, and testing of the feedlines was performed in-house at MSFC. As each feedline was received, it was hydrostatically tested at 50 psi and inspected visually for leakage. If no gross leakage was detected, nondestructive evaluation (NDE) of the feedlines was performed by the NDE team at MSFC and consisted of flash thermography. Upon completion of NDE, the feedlines were given to the

mechanical design group at MSFC for instrumentation, cyclic cryogenic, and pressurization testing. After this series of tests, a few feedlines were hydrostatically burst while the others were destructively tested for microcracking. The strength analysis group at MSFC performed an analysis of the feedlines and the results were compared to the measured values obtained in the full-scale tests.

A damage tolerance subtask was also undertaken in this study. It consisted of testing laminates made from the four manufacturing processes for damage resistance and permeability after impact testing. Full-scale test articles were also impacted to see at what threshold leakage would occur.

2. TEST ARTICLE

Within this task, a common test article was chosen to evaluate the different material systems and manufacturing methods. A drawing of the test article is shown in figure 1.

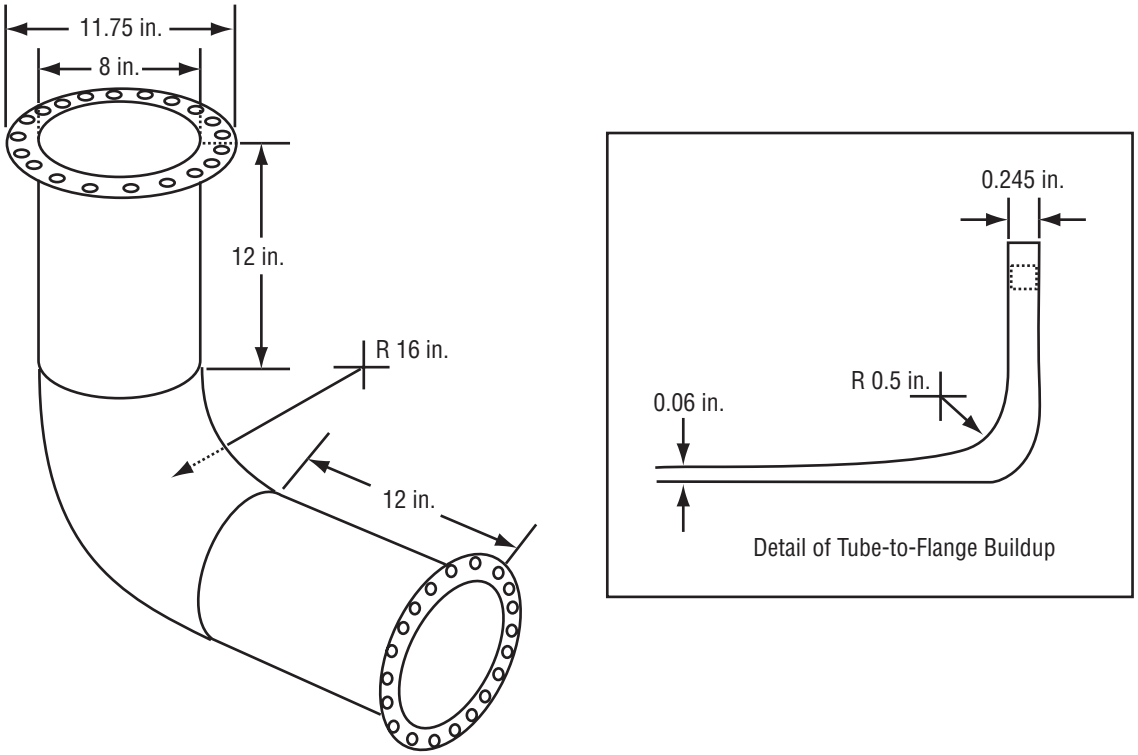

Figure 1. Drawing with dimensions of the common test article.

The flanges on the ends are integral to the tube; i.e., the test article is one piece. An elbow section was chosen to demonstrate a more complex geometry than a simple straight tube. The thickness dimensions of the tube's walls are approximate since the final dimensions would be heavily dependent on the manufacturing process used.

At the beginning of the task, four different manufacturing methods were chosen for comparison. These methods are (1) conventional HLU and autoclave cure, (2) SARTM, (3) electron beam cure, and (4) TTL. Of these four techniques, test articles were made from three, although all types underwent some coupon-level material testing. The electron beam cure technique never produced a full-scale test article. The details of the material and layup of the other three follow.

2.1 Conventional Hand Layup

The most common method of producing composite parts for space hardware is HLU of prepreg material with an autoclave cure. This was done at MSFC's Productivity Enhancement Center (PEC). The material selected for this manufacturing method was IM7 carbon fiber with a toughened epoxy resin. Two types of resin were used in this study. One was from Bryte Technologies, designated EX1522; the other was from Hexcel®, Incorporated, designated 977–6. The fiber architecture was a five-harness satin weave. The resin was impregnated into this and B-staged to produce the prepreg material used. The layup sequence for the test article was [0/90,±45,±45,0/90] with buildups into the flanges. The prepreg was cut to size and hand-laid on a male tube to form the part (fig. 2). Once the part was laidup, it was bagged and autoclave cured at 350 °F.

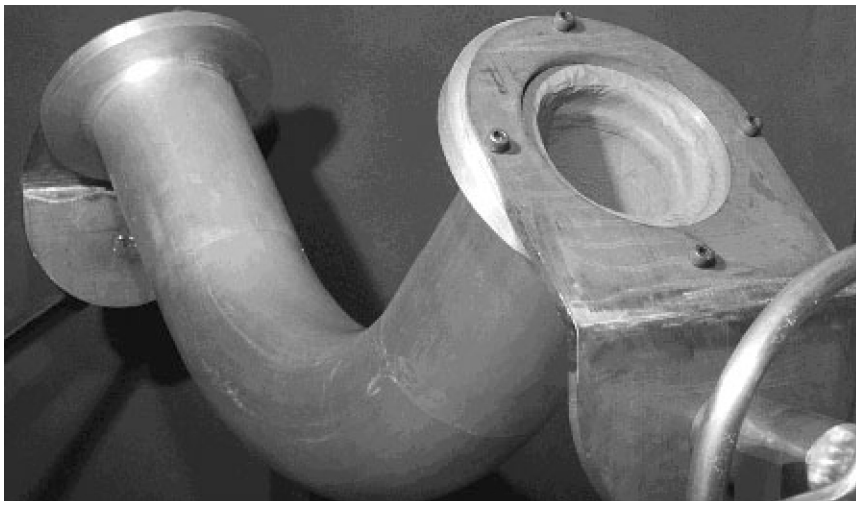

Figure 2. Reusable tool used for HLU.

Eight tubes were made using this technique. Other tubes were made with different prepreg material, but they will not be included in this report. A photograph of a completed test article manufactured via HLU is shown in figure 3. The total weight of the feedline was 6.7 lb. The outside surface is not smooth since it was simply bagged and not against a tool. A closer view of the flange buildup area is given in figure 4. Some creasing in the region between the tube and flange sections can be seen. This was typical of all of the feedlines manufactured in this way. It is suspected that this is just a cosmetic anomaly and will not adversely affect the performance of the feedline.

Figure 3. Completed test article manufactured by HLU.

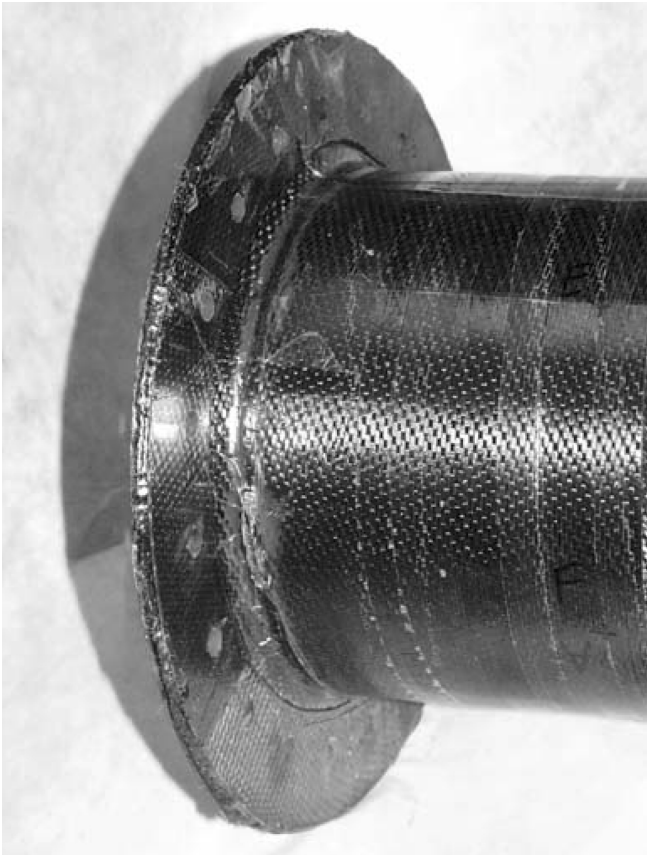

Figure 4. View of flange area on a feedline manufactured via HLU.

The microstructure of the feedline in the acreage of the feedline is shown in figure 5. Excellent ply consolidation is evident. The relatively small resin-rich areas observed for a five-harness weave prepreg also notes good compaction.

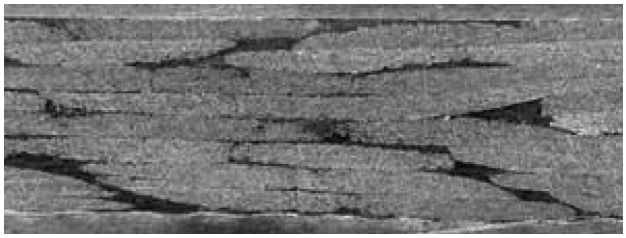

(a)

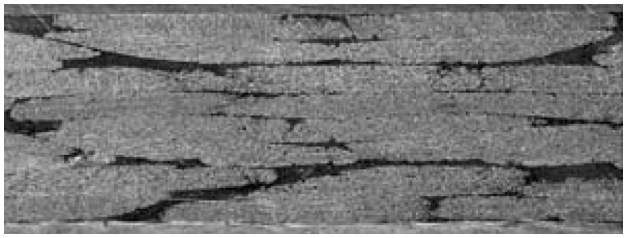

(b)

Figure 5. Microstructure of feedline manufactured via HLU:
(a) Longitudinal view and (b) radial view.

2.2 Solvent-Assisted Resin Transfer Molding

Another method used to make test articles was performed at NASA's GRC and consisted of SARTM. This technique involved drawing the resin up through a fiber preform of the part and then autoclave curing. The fiber preform is braided with IM7 carbon fiber into the geometry of the final part. This preform is placed over a male tool and a female mold placed over the preform. Resin is drawn through the preform by placing a vacuum on one end of the elbow and resin with solvent added at the other end. Once the resin has impregnated the entire perform, the part is autoclave cured. The solvent is added to the resin to lower its viscosity to aid in the wetting out of the preform.

The resin used to make the test article in this study was PR 520, a toughened epoxy manufactured by Hexcel. However, test panels made with SI–SE–1 and Cycom® 823 epoxies were tested during the material characterization and damage tolerance phases of this program. A completed feedline manufactured via SARTM is shown in figure 6. A closer view of the flange area is given in figure 7. Both the inside and outside surfaces of the tube are smooth since they are both tool sides.

Figure 6. Completed test article manufactured via SARTM.

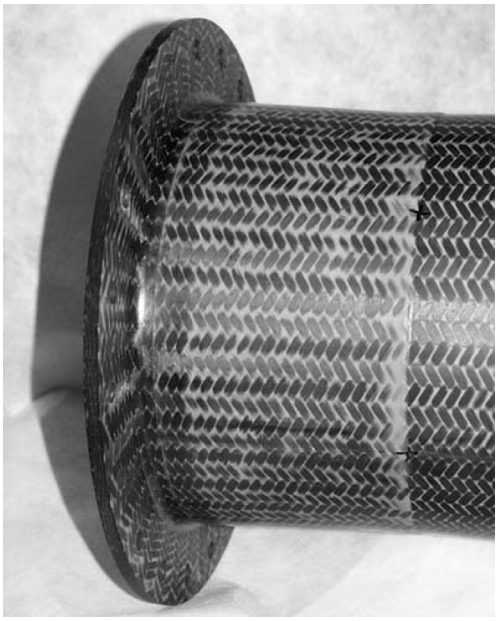

Figure 7. View of flange area of a feedline manufactured via SARTM.

The microstructure of the feedline in the acreage area is shown in figure 8. As with the feedline manufactured via HLU, this feedline also demonstrated excellent consolidation and compaction with no voids. The solvent-assisted resin did an excellent job of wetting out all of the fibers in the preform.

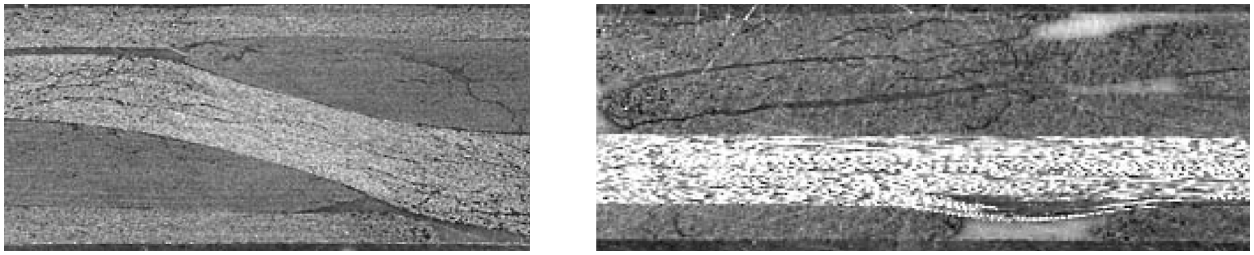

(a) (b)

Figure 8. Microstructure of feedline manufactured via SARTM:
(a) Longitudinal view and (b) radial view.

2.3 Thermoplastic Tape Laying

Another method used to manufacture test articles was TTL. This method consists of laying tape ≈0.25 in. wide over a male mold and melting it into place as it is put down using a robotic head. The layup sequence of the plies that were built up was $[0,90,+45,–45]_S$ with the 0° direction defined along the axis of the tube. A photograph of a test article being manufactured using this method is shown in figure 9. For this process, IM7 carbon fiber was used with a polyetheretherketone (PEEK) resin.

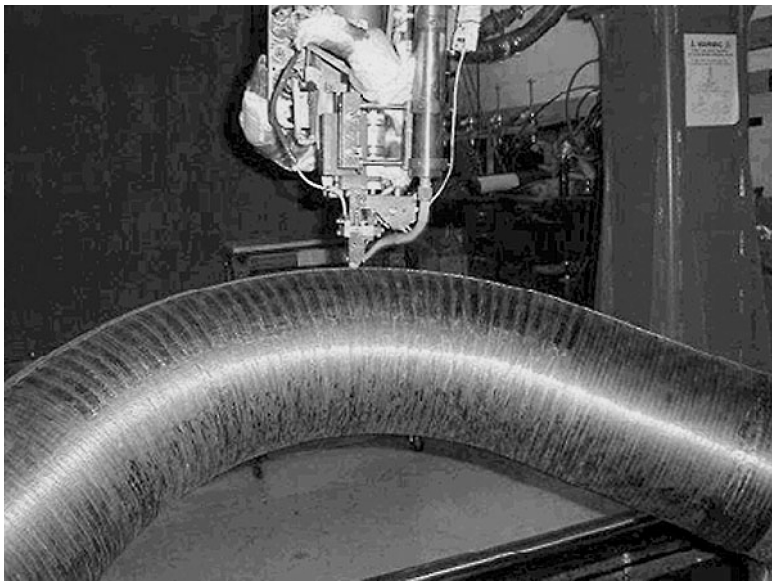

Figure 9. A test article being manufactured by TTL.

Figure 10 shows a completed feedline manufactured by TTL. A closer view of the flange area is given in figure 11. This area is particularly rough with obvious areas of nonconsolidation visible from the surface. This was of great concern since it could facilitate leaks and compromise the structural integrity of the feedline. A view of the microstructure in the acreage of the feedline is given in figure 12. Poor consolidation with large areas of delamination can be seen. The thermoplastic tape apparently was difficult to compact by the robotic head.

Figure 10. Completed test article manufactured via TTL.

Figure 11. View of flange area of a feedline manufactured via TTL.

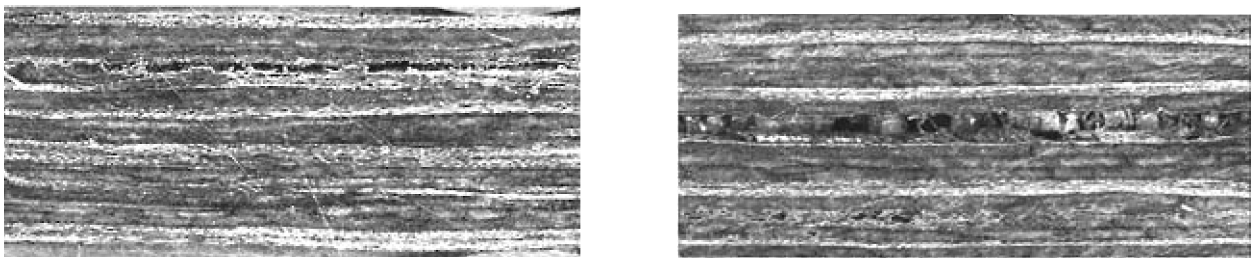

(a) (b)

Figure 12. Microstructure of feedline manufactured via TTL:
(a) Longitudinal view and (b) radial view.

3. TESTING

Section 3 outlines the tests performed during this study. Results are presented in section 4.

3.1 Nondestructive Evaluation Testing

The feedlines were inspected using flash thermography, an NDE technique. Flash thermography consists of hitting the test article with a pulse of heat and then monitoring the release of the heat with an infrared camera. Areas that have anomalies will give off heat at a different rate than the rest of the tube, thus identifying the location and general shape of possible defects. A sample picture of a thermography image is shown in figure 13. In this figure, it can be seen that an anomaly appears (which turned out to be plastic tape).

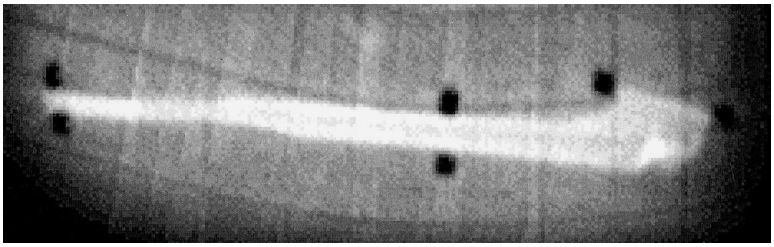

Figure 13. Flash thermography image showing foreign object (plastic tape) inclusion.

The dark spots around the perimeter of the defect in figure 13 are foil markers used to help identify locations on the thermograms. Each test article was marked off with an array of foil markers as shown in figure 14. This produced a grid pattern so each thermogram could be identified. For example, the dark gray shaded area in figure 14 would be designated “position B2” and the light gray shaded area “position E12.” Due to the bend in the article, there is a smaller distance between the flanges along the inside radius of the tube; thus, there are only 11 areas along the inside radius versus 13 areas along the outside radius. A sample thermogram with no anomalies is shown in figure 15.

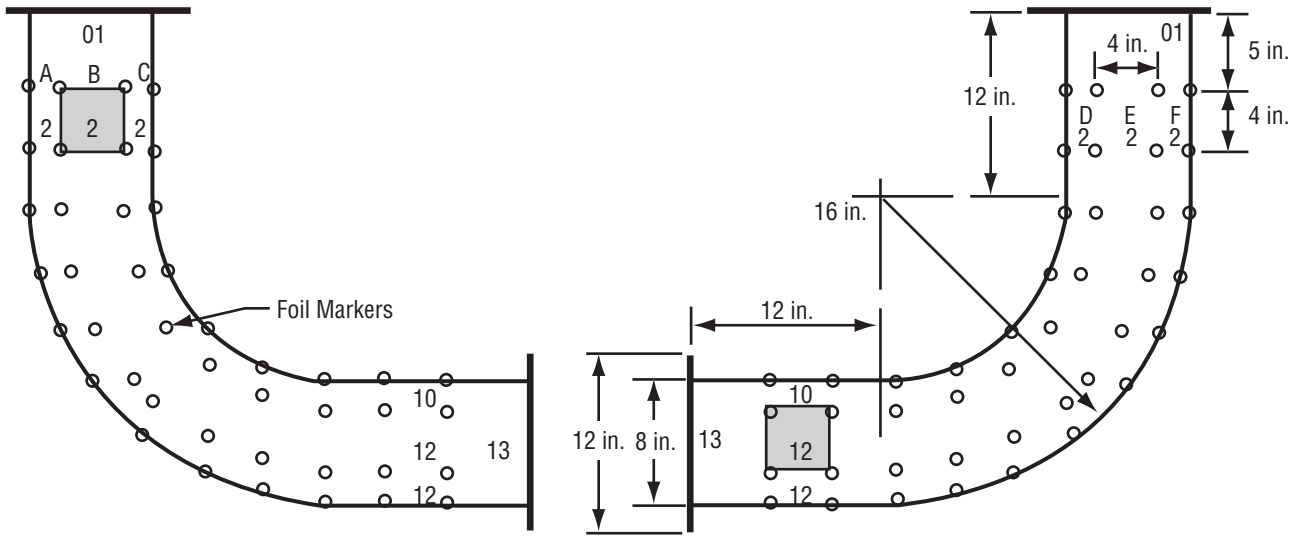

Figure 14. Schematic showing placement of array of foil markers.

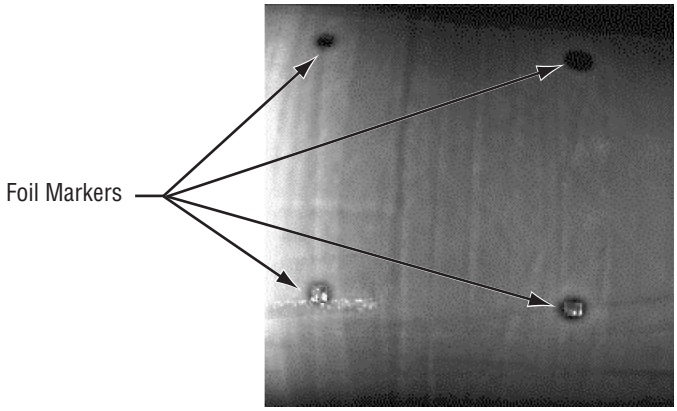

Figure 15. Thermograph of position E12 on test article No. 3.

3.2 Proof Testing

A hydrostatic proof test was performed on each test article to verify its integrity. The test articles were proof pressure tested to 150 psi. The pressure was maintained for 60 sec and then reduced to zero psi. This was repeated for a total of five cycles. The test article was visually observed for any leaks during the test.

3.3 Leak Testing

Once proof testing was completed, the next series of tests performed were leak checks at 50 psi using gaseous helium (GHe). The test article was enclosed in a bag (excluding the flange bolts and seal joint) to capture any GHe leaking through the parent material. A probe connected to a helium (He) mass spectrometer was inserted into the bag to sense for any He leakage. The test article sat for 10 min before a leakage reading was recorded. If leaks were found, the test article was set aside and not used for cryogenic testing. The tubes with leaks were taken to the damage tolerance facility in MSFC's PEC and examined further to determine the possible cause of the leaks. Figure 16 shows a bubble-leak detect solution being applied to one of the test articles manufactured by HLU. In this particular feedline, a line of small leaks was apparent.

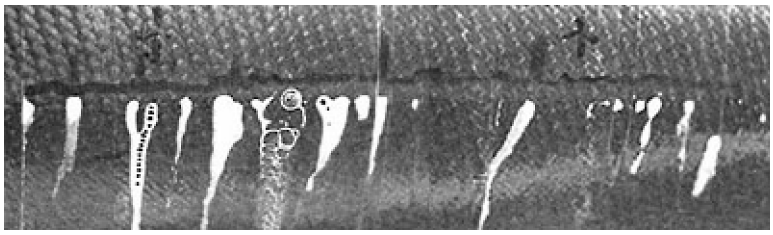

Figure 16. Leak as detected by bubble-type solution in a test article.

3.4 Cryogenic Testing

The cryogenic testing series was performed on a select number of feedlines that had passed the proof and leak tests. These feedlines were tested at MSFC's test stand 300 and an outline of the testing performed is given in table1.

Table 1. Cryogenic testing series.

Test No.	Test
1	Leakage
2	10 Thermal/Pressure Cycles with LN_2
3	Leakage
4	15 Thermal/Pressure Cycles with LH_2
5	Leakage

A brief explanation of each of these tests follows:

- Leakage: A pretest and posttest leak check was done on each test article. A pretest leak check was performed after the test article was installed in the test stand. The test article was pressurized to 50 psig with GHe and checked for leaks using leak check solution. A posttest leak check was also performed on the test article after the 10 liquid nitrogen (LN_2) cycle tests and the 15 LH_2 cycle tests. This posttest leak check was done prior to removal of the test article from the test stand and was done in the same manner as the pretest leak check. If the test article passed the posttest leak check, a more-refined leak check was performed using a GHe mass spectrometer to quantify any leakage. This refined leak check was performed as described in section 3.3.

- Thermal/Pressure Cycle Test with LN_2: Each test article was subjected to 10 pressure and thermal cycles. The pressure was cycled from 0 to100 psi. The temperature was cycled from LN_2 temperature to 140 °F. LN_2 was flowed through the test article at ≈10 psi to chill it. Heated gaseous nitrogen (GN_2) was flowed through the test article to heat it. A typical thermal/pressure cycle was performed as follows: Starting at ambient temperature and pressure, the test article was chilled with LN_2 until the skin temperature reached a steady-state temperature. A dwell time of 5 min at the steady-state temperature condition was maintained. While cold, the pressure inside the test article was increased to 100 psi and dwelled for 1 min at the steady-state pressure condition. The pressure was then vented and the test article was warmed to 140 °F temperature using heated GN_2, and dwelled for 5 min at the steady-state temperature condition. The test article was chilled again and the testing was repeated for the total number of cycles required.

- Leakage: Like above.

- Thermal/Pressure Cycle Test With LH_2: Performed 15 pressure and thermal cycles on the test article using LH_2. This test was run in the same manner as the LN_2 test above.

- Leakage: Like above.

- The following instrumentation was used for each test article:

  – 17 biaxial strain gauges.

  – 5 skin temperature sensors.

  – Fluid temperature sensors located on the facility immediately upstream and downstream of the test article.

  – One internal pressure measurement located on the facility.

  – Video coverage of test article.

The location of the 17 strain gauges is shown in figure 17.

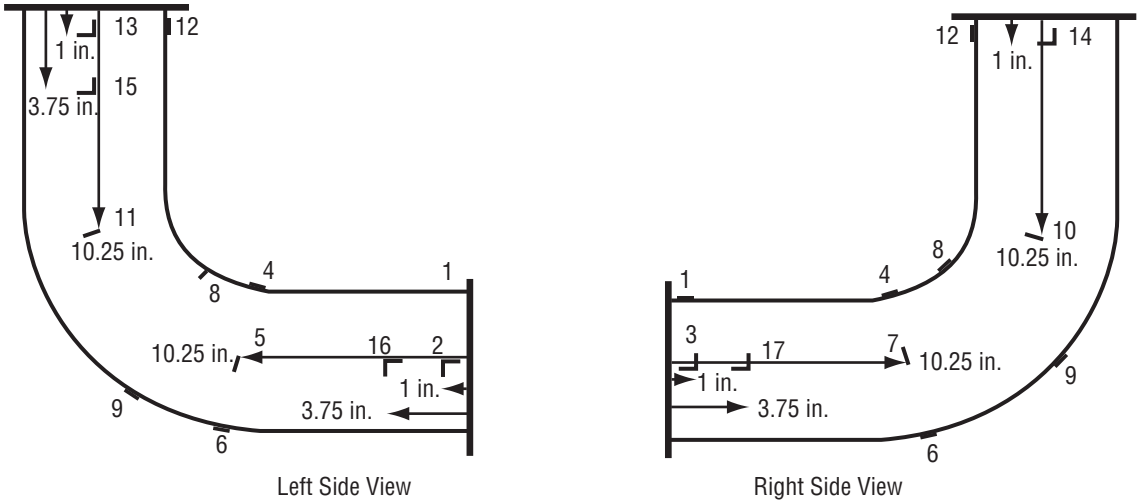

Figure 17. Location of 17 biaxial strain gauges on the test articles.

3.5 Burst Pressure Testing

A hydrostatic burst pressure test was performed to determine strain versus pressure until failure. Each test article was filled with water and pressure was slowly increased until failure. The test was done at ambient temperature. Strain at each of the 17 gauges shown in figure 17 was recorded as well as internal pressure. Video of the failure was also recorded. The test articles were mounted such that each flange was rigidly fixed and immovable.

3.6 Damage Tolerance

All of the candidate materials were screened for damage resistance/damage tolerance. Flat panels of the candidate materials were impacted with a drop-weight apparatus and assessed for damage and resulting permeability. To assess damage, the specimens were visually examined and the damage digitally documented. The specimens were then sectioned and polished for a through-the-thickness assessment of the damage imparted by the impact event. This damage was enhanced with an ultraviolet (UV) dye solution and then photographed under a UV light source to highlight the damage. Some specimens were tested for permeability after impact.

4. RESULTS

Section 4 presents results of the NDE, leak, cryogenic, burst pressure, and damage tolerance testing performed during the course of this study.

4.1 Nondestructive Evaluation Testing

The results of the flash thermography testing are quite voluminous with a digital image of each grid on each test article taken for 72 images per tube. Only indications of significance will be presented in this section.

4.1.1 Test Articles Manufactured via Hand Layup

Eight HLU feedlines that were autoclave cured were inspected using flash thermography. Feedline HLU–1 showed no anomalies. For feedline HLU–2, only one major indication was found. The abnormality appears hot (white) which would indicate a void or inclusion of some material that blocks the flow of heat into the tube. The thermogram for this anomaly is given in figure 18.

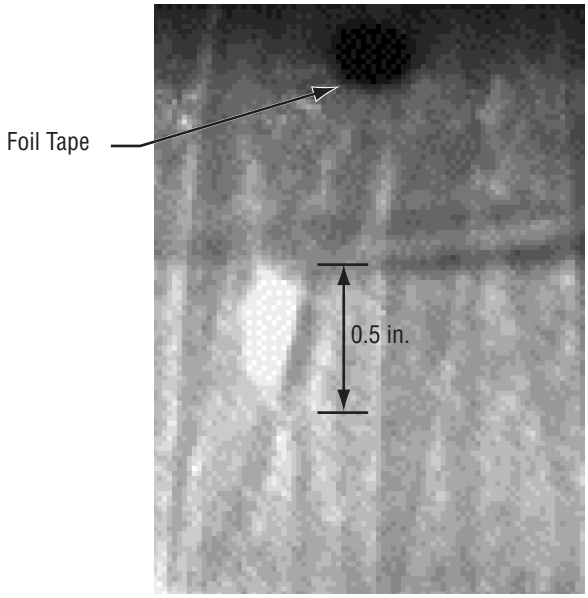

Figure 18. Anomaly noted on thermograph of feedline HLU–2.

A large inclusion was found on the inner radius of feedline HLU–3. The thermographs are shown in figure 19. Since this anomaly was so large, the feedline was scrapped for subsequent testing. This provided an opportunity to dissect the feedline to determine the cause of the anomaly. Upon sectioning, it was found that the anomaly was a piece of plastic tape under the innermost ply of prepreg. This can be clearly seen in figure 20.

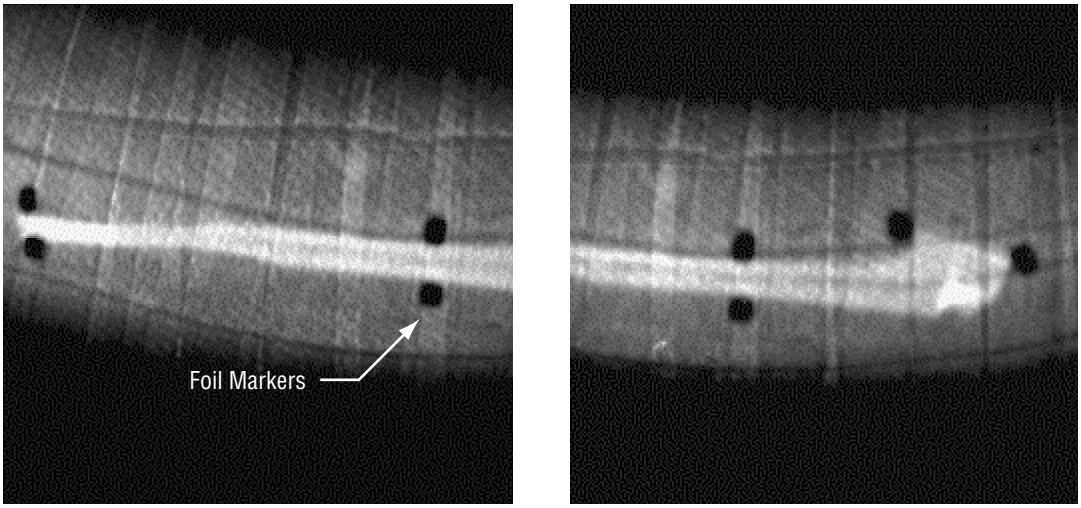

Figure 19. Large inclusion found on feedline HLU–3.

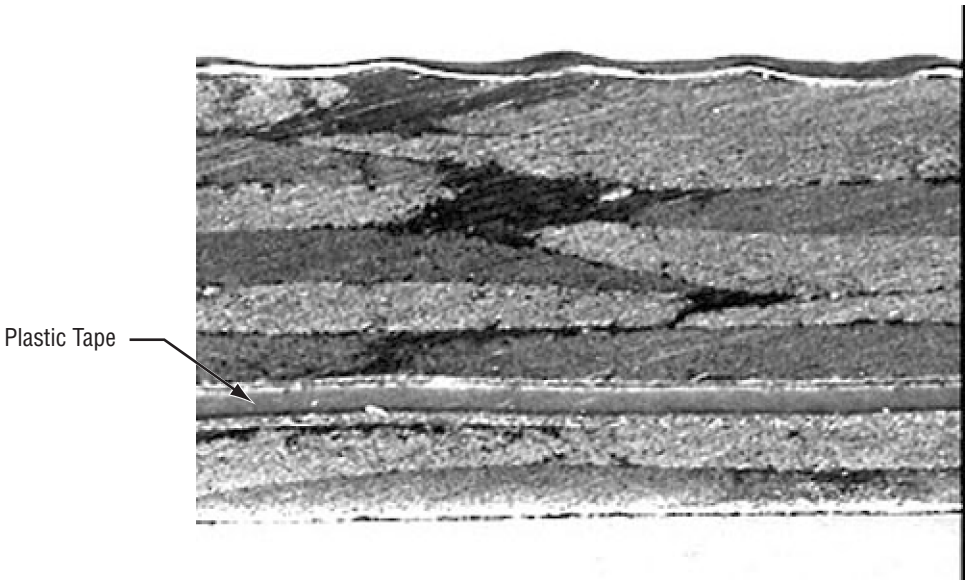

Figure 20. Cross section of plastic tape causing anomaly in figure 13.

In feedline HLU–4, dark bands found throughout the acreage of the tube (both circumferential and axial), most likely indicate ply overlaps and resin pockets. In figure 21, these dark bands are illustrated along with an inclusion. A delamination was found below a ply splice in the tube acreage. Visual inspection of the region found a surface crack along the upper edge of the indication at the ply splice.

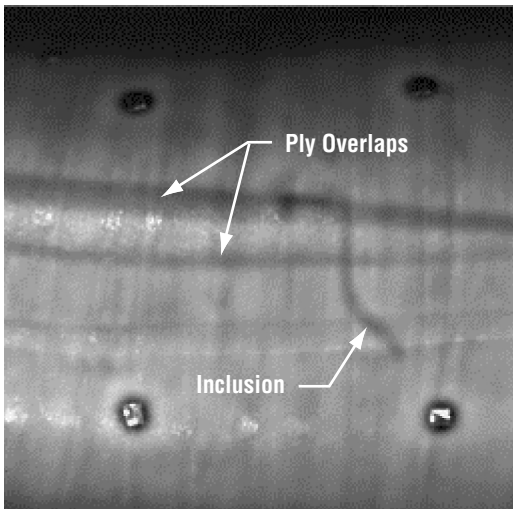

Figure 21. Dark regions and anomaly found in tube HLU–4.

Feedline HLU–5 showed numerous indications as outlined in figures 22a–22g.

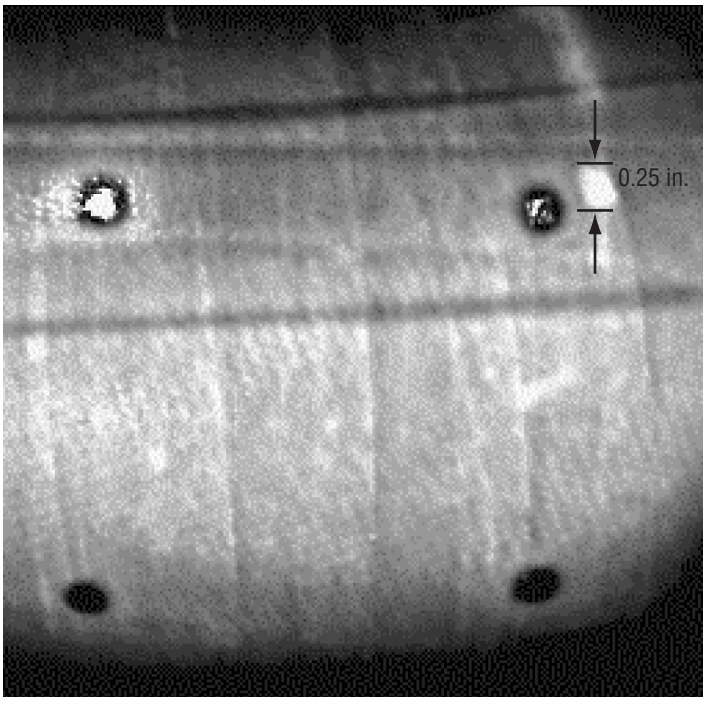

Figure 22a. No surface features, but strong thermal indication. Possible “thin film” inclusion.

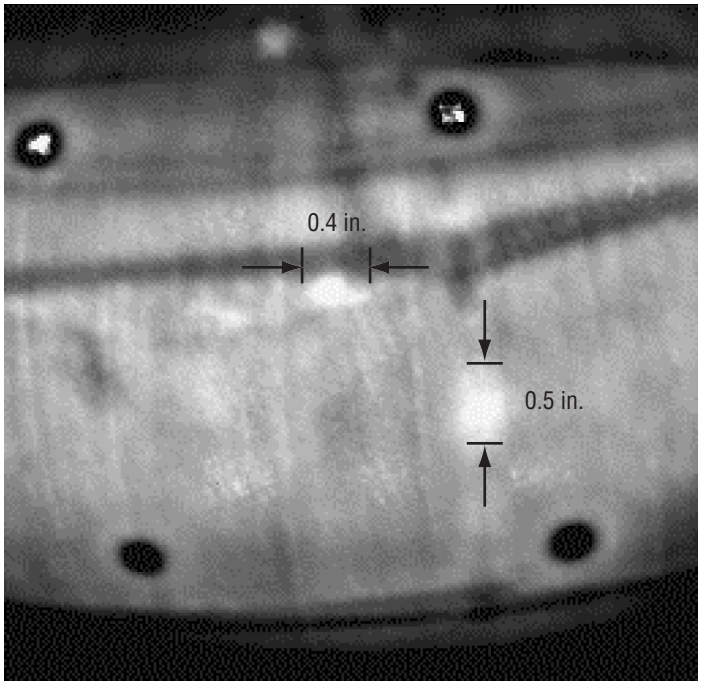

Figure 22b. No surface features. Unknown source.

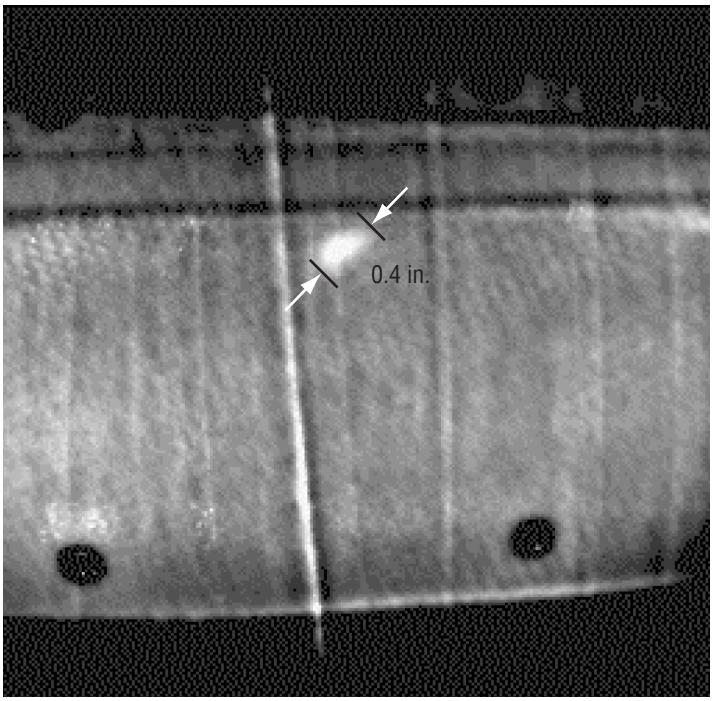

Figure 22c. No surface features but strong thermal indication. The blurred edges may indicate that this is a delamination from impact.

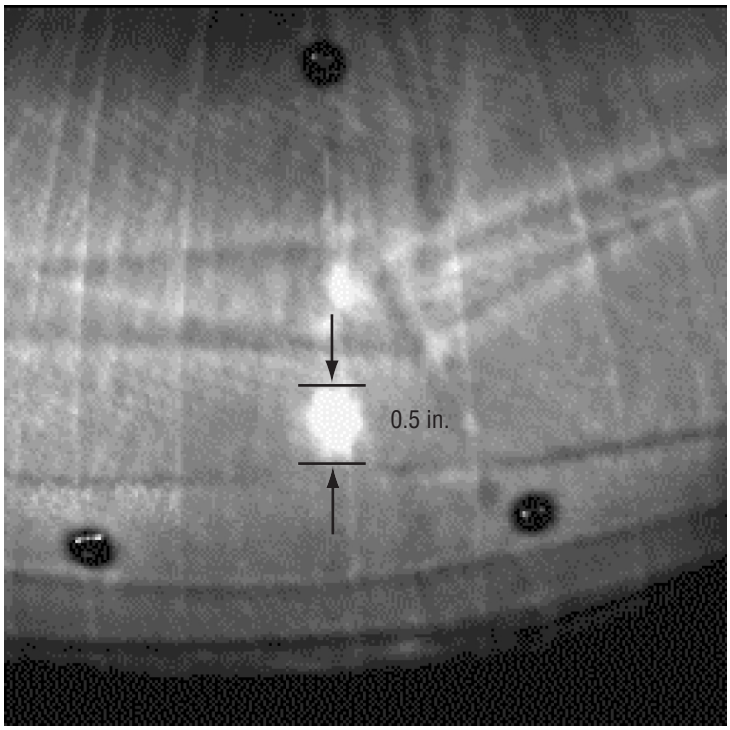

Figure 22d. A bump is visible on the surface indicating an inclusion with possible internal void.

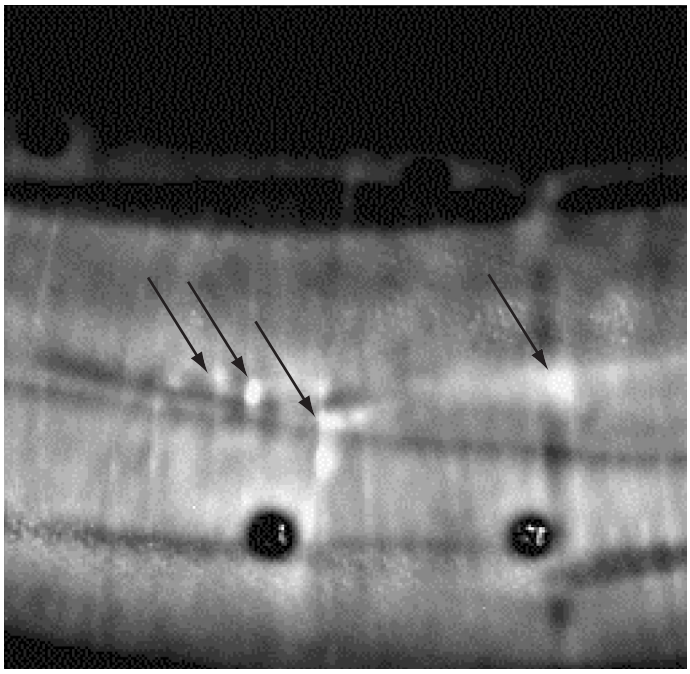

Figure 22e. The surface of the tube shows signs of overworking during fabrication. These regions may be thin, resin-starved zones (indicated by the arrows).

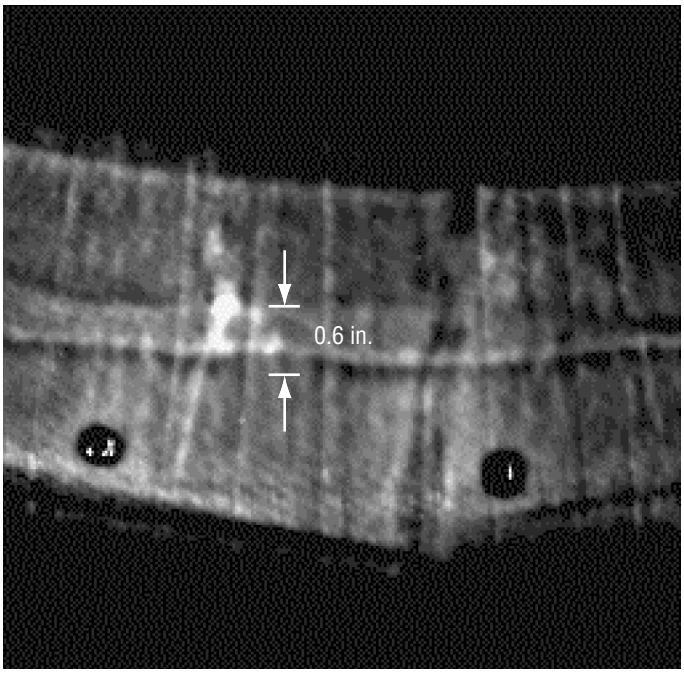

Figure 22f. The surface of the tube has a small bump, which would indicate an inclusion.

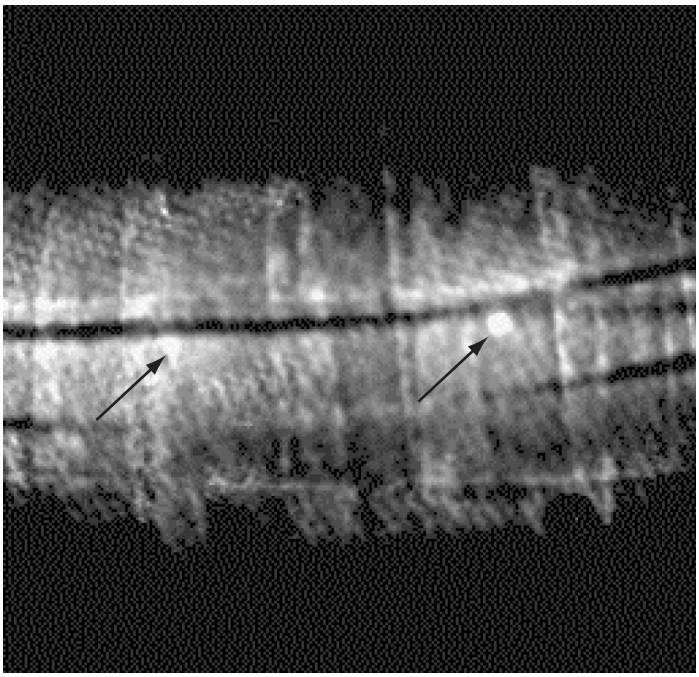

Figure 22g. Possible voids along a seam.

For feedline HLU–6, indications 1, 2, and 3 in figure 23 appear on the surface as small bumps and may be inclusions or ply wrinkles with embedded voids.

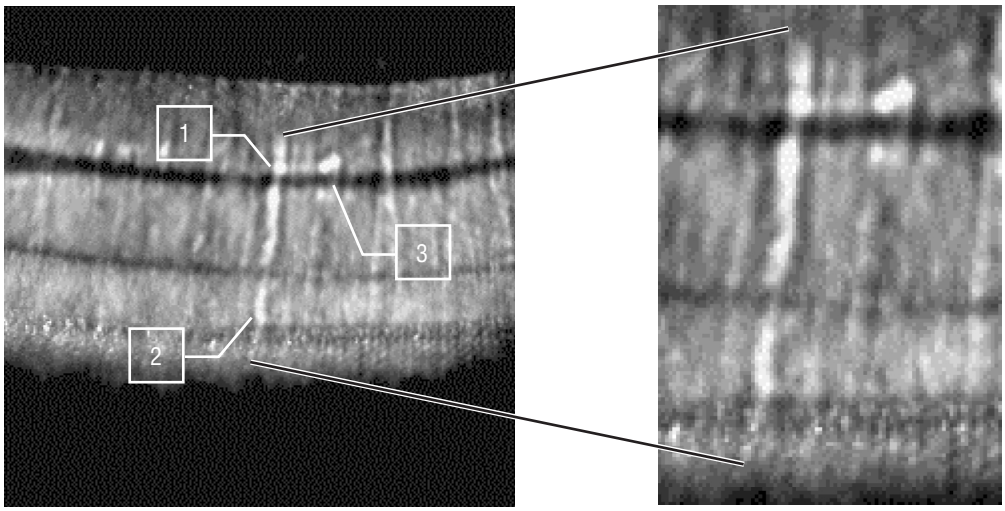

Figure 23. Anomalies on feedline HLU–6.

Feedline HLU–7 appears to have been scuffed and the indication shown in figure 24 is visible as a scratch with exposed fibers. In addition, on feedline HLU–7, a faint surface ripple is visible, indicating a deeply embedded inclusion. The thermograph is shown in figure 25.

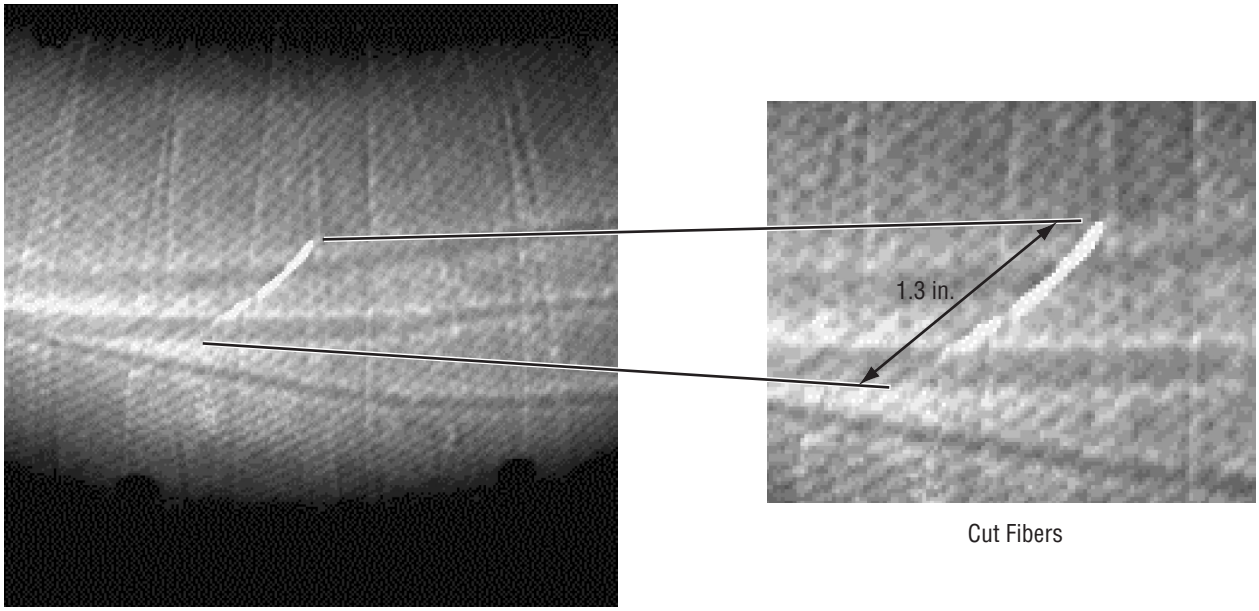

Figure 24. Thermography image of scuff on feedline HLU–7.

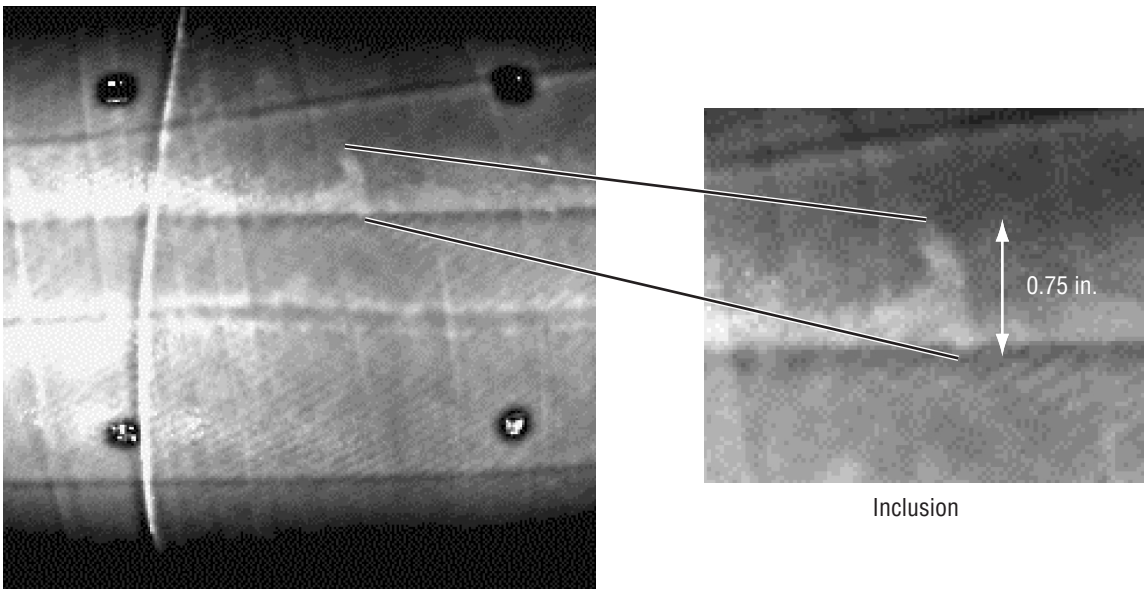

Figure 25. Thermograph of possible deep inclusion on feedline HLU–7.

On feedline HLU–8, three small thermal abnormalities were detected as shown in figure 26. The size of each indication was <0.25 by 0.5 in. At region A3, the indication correlates with a surface crack. At position F3, the indication appears to be within the laminate. At position B12, the indication is visible on the surface as a scratch.

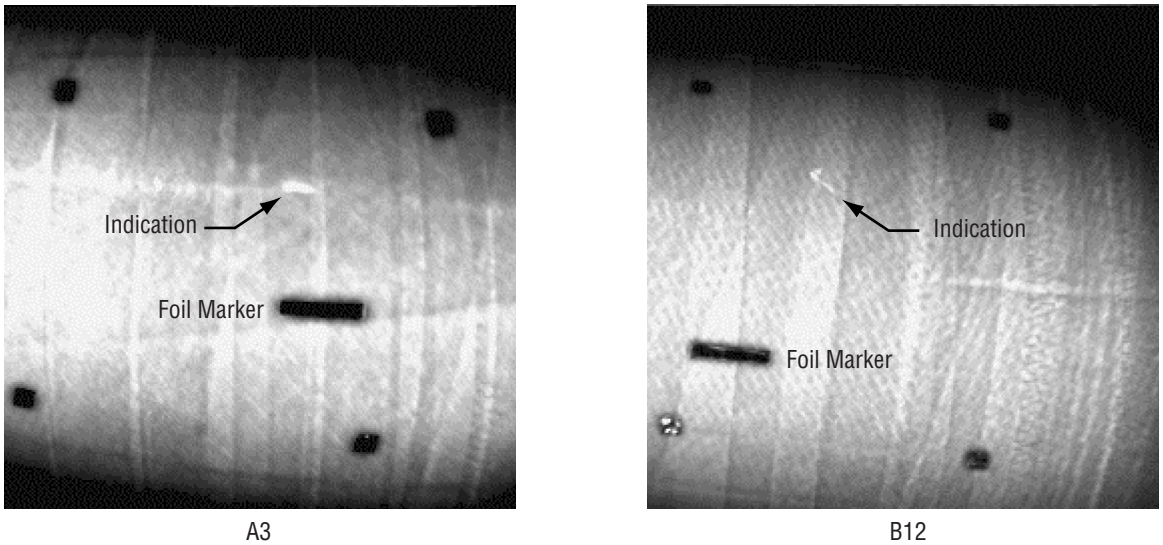

Figure 26. Anomalies in feedline HLU–8.

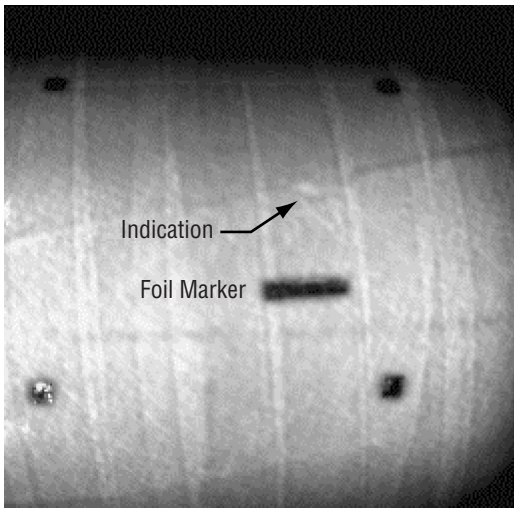

F3

Figure 26. Anomalies in feedline HLU–8 (continued).

4.1.2 Test Articles Manufactured via Solvent-Assisted Resin Transfer Molding

Four feedlines, manufactured using SARTM, were inspected using flash thermography. Feedline SARTM–1 showed no anomalies. Feedline SARTM–2 showed a ring of thinning that was detected on the inside of the tube ≈12 in. in from the flange. This is shown in figure 27.

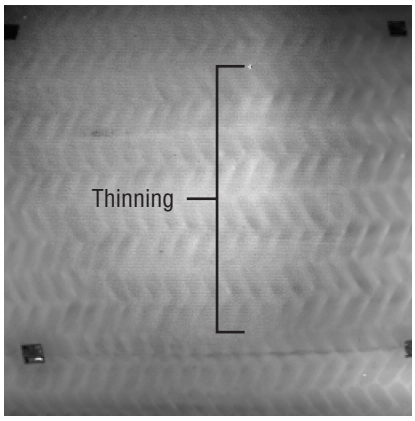

Figure 27. Thermograph showing thinning in feedline SARTM–2.

Feedline SARTM–3 showed the same type of thinning at the same location as feedline SARTM–2. A thermograph is presented in figure 28.

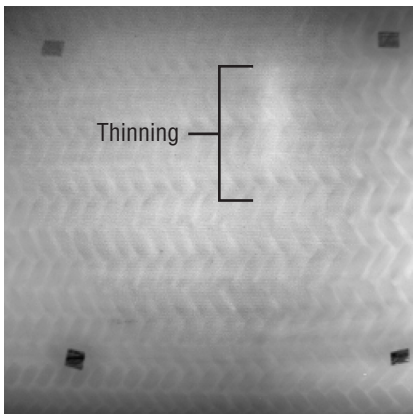

Figure 28. Thermograph of thinning in feedline SARTM–3.

Feedline SARTM–4 showed no major anomalies.

4.1.3 Test Articles Manufactured via Thermoplastic Tape Laying

Four feedlines manufactured via TTL were inspected using flash thermography. For feedline TTL–1, the acreage of the tube appears to have many highly porous/low consolidation regions as indicated by the many bright patches in the images. The bright regions in the flange thermograms coincide with missing plies on its back surface. The fillet also shows many low consolidation/highly porous regions. Sample thermograms showing these voids are given in figure 29.

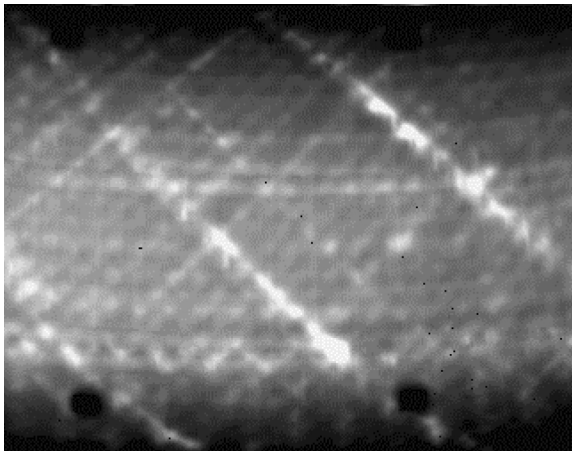

Acreage

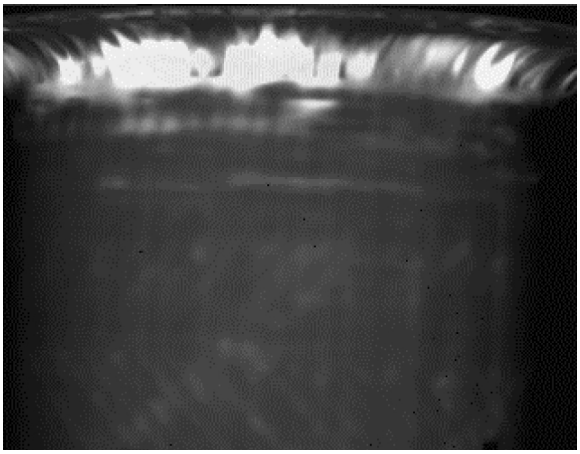

Flange Buildup

Figure 29. Sample thermograms from feedline TTL–1 showing regions where the tape was not well consolidated in acreage and voids in flanges.

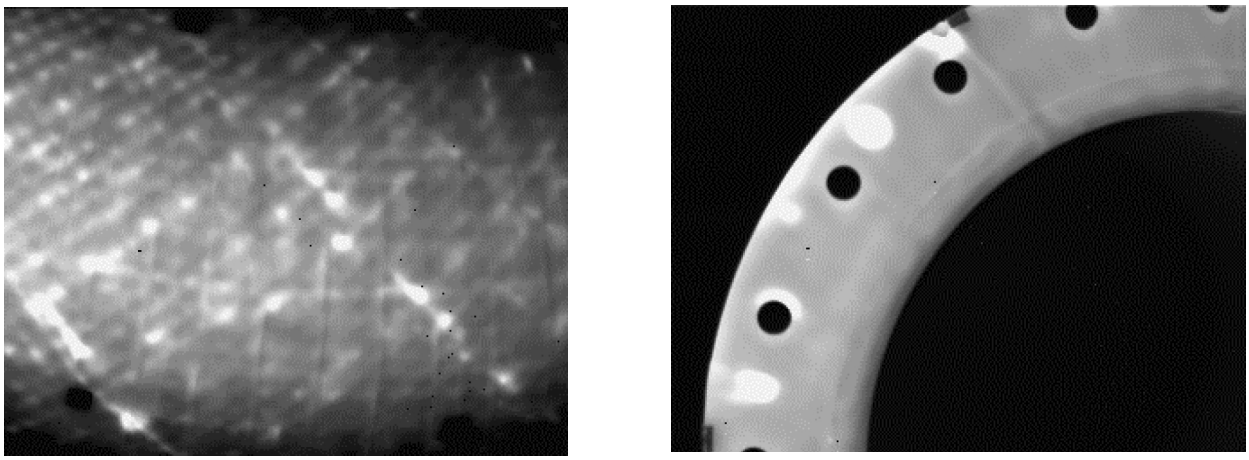

Acreage Flange

Figure 29. Sample thermograms from feedline TTL–1 showing regions where the tape was not well consolidated in acreage and voids in flanges (continued).

Feedlines TTL–2, TTL–3, and TTL–4 all demonstrate the same type of indications as feedline TTL–1.

4.1.4 Test Articles Manufactured via Electron Beam Cure

No test articles manufactured by electron beam curing were produced for this study; therefore, no testing was performed.

4.2 Proof and Leak Testing

All of the feedlines underwent a hydrostatic proof test and leak test before advancing to cryogenic testing. Those tubes that leaked were taken to the damage tolerance laboratory for more detailed examination and documentation. This section presents the results of these tests.

4.2.1 Test Articles Manufactured via Hand Layup

Of the eight test articles manufactures by HLU, two leaked prior to cryogenic testing. Feedline HLU–5 had two areas of linear pinhole leaks and feedline HLU–6 leaked at several sites. Figure 30 shows the two areas of linear pinhole leaks in feedline HLU–5. The tube was pressurized with 20 psi of GHe and a leak detect solution was squirted on the outside. The resulting trail of very small bubbles indicates very small leaks.

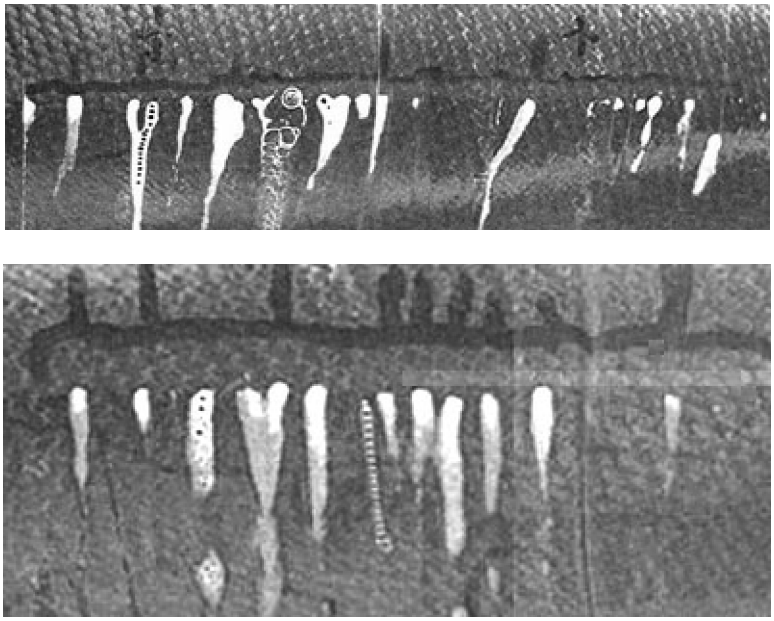

Figure 30. Two areas of pinhole leaks on feedline HLU–5.

Figure 31 shows some of the leaks on feedline HLU–6. Note that these leaks form larger bubbles than those on feedline HLU–5 (as shown in fig. 30). This indicates larger "holes," as does the fact that the pictures in figure 31 were taken with the tube at only 3.5 psi. The area of leaks on feedline HLU–6 was marked off into a grid pattern with each grid numbered so the leaks could be better identified.

Figure 31. Samples of leak areas on feedline HLU–6.

Figure 31. Samples of leak areas on feedline HLU–6 (continued).

4.2.2 Test Articles Manufactured via Solvent-Assisted Resin Transfer Molding

Of the four feedlines manufactured by SARTM, two leaked prior to cryogenic testing. Feedline SARTM–1 demonstrated three areas of leakage and feedline SARTM–3 showed one area of leakage. Figure 32 shows the three leaks in feedline SARTM–1. One of the leaks is large compared to the other two. The feedline was pressurized at 5 psi when the photograph was taken.

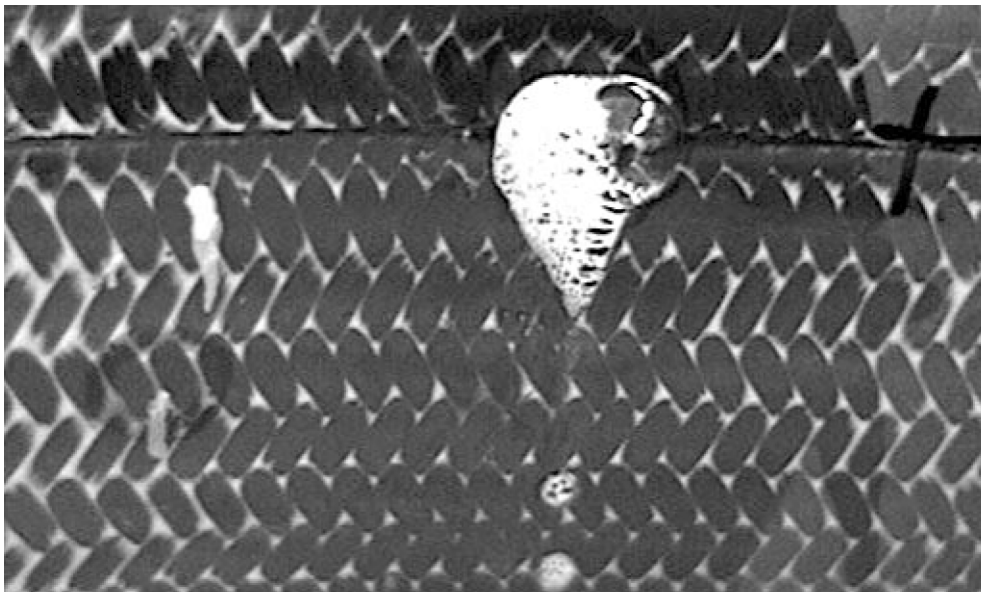

Figure 32. Feedline SARTM–1 showing three leak paths.

Figure 33 shows the one leak found in feedline SARTM–3. Due to the large size of the bubbles, the leak is significant. The feedline was pressurized at 2.5 psi when this photograph was taken.

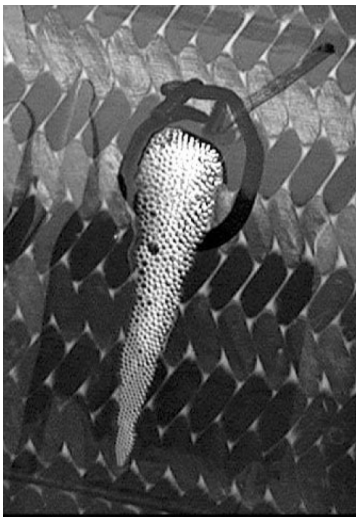

Figure 33. Feedline SARTM–3 showing one large leak path.

Since these feedlines would not undergo any further testing, they were sectioned at the areas of leakage and photomicrographs taken. Figure 34 shows the cross section of feedline SARTM–1 in which an air bubble appears to be responsible for the leakage seen. Figure 35 shows the cross section of feedline SARTM–3. A small region of the preform is resin starved and provided the large leak path seen.

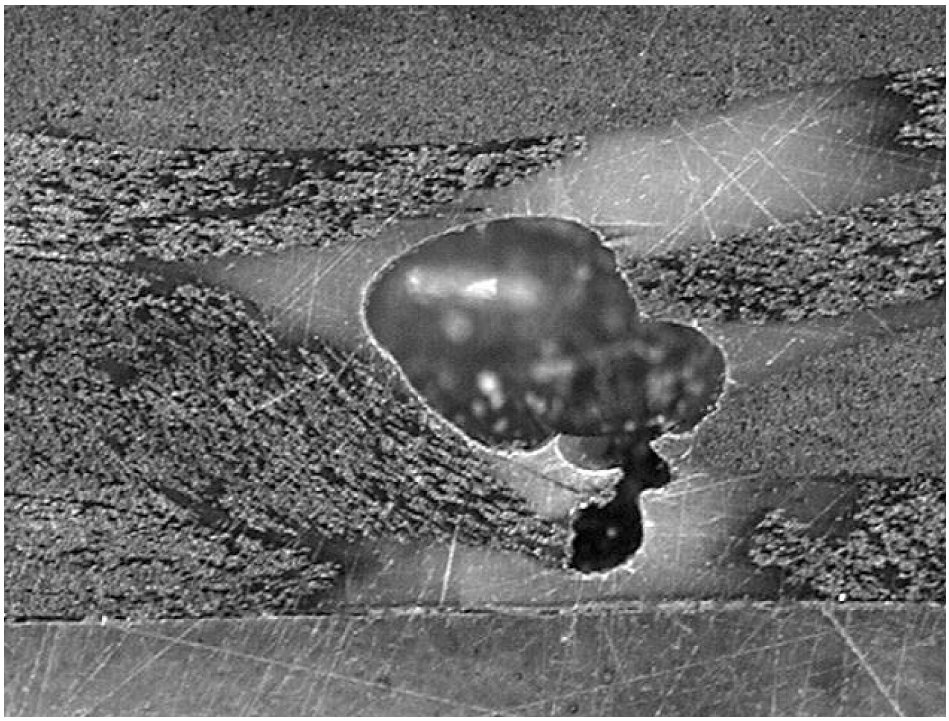

Figure 34. Cross section of leak area on feedline SARTM–1.

Figure 35. Cross section of leak area on feedline SARTM–3.

4.2.3 Test Articles Manufactured via Thermoplastic Tape Laying

Four feedlines manufactured via TTL were leak tested. All four feedlines showed leakage around the flange buildup area. Figure 36 shows the leakage on feedline TTL–2. The feedline was pressurized at 5 psi for these leak tests. Some of the leaks are very small while others are larger as evidenced by the larger bubbles forming.

Figure 36. Feedline TTL–2 showing ring of leakage around flange buildup area.

These feedlines also showed leakage at the flange transition areas. Some of these leaks were so exceptionally large that maintaining pressure in the feedline was difficult. Figure 37 shows the flange on feedline TTL–3. The tube was only at 2 psi and it can be seen that the leak detect solution is being splattered into the air since the leak is of such a gross nature.

Figure 37. Flange area of feedline TTL–3 showing gross leakage.

4.3 Cryogenic Testing

Only the feedlines that did not leak were accepted for cryogenic testing as outlined in section 3.4. None of the TTL feedlines met these criteria. Only HLU and SARTM feedlines (those that did not leak) could be tested. Each feedline was installed in the test facility with one flange end firmly fixed and the other flange end free. These end conditions allowed for movements in the test setup due to the temperature changes from the test fluid. Each feedline was insulated using a foam clamshell-type arrangement. This allowed for ease of installation, removal, and reuse of the insulation. Figure 38 shows a photograph of feedline HLU–2 insulated and installed in test stand 300 for cryogenic testing and a photograph of the feedline with half of its insulation removed and some of the instrumentation visible. The mating flanges to the composite feedline were made of stainless steel. Differences in the coefficient of thermal expansion between the two different flange materials were considered during selection of the proper seal for the flanges. The composite flange was designed with a flat face and the mating stainless steel flange was machined with a seal groove in its face. An Omniseal®, part No. 348–374–0101, manufactured by Saint-Gobain Performance Plastics, was selected to seal the flanges. The following presents the results of the cryogenic tests with LN_2 and LH_2.

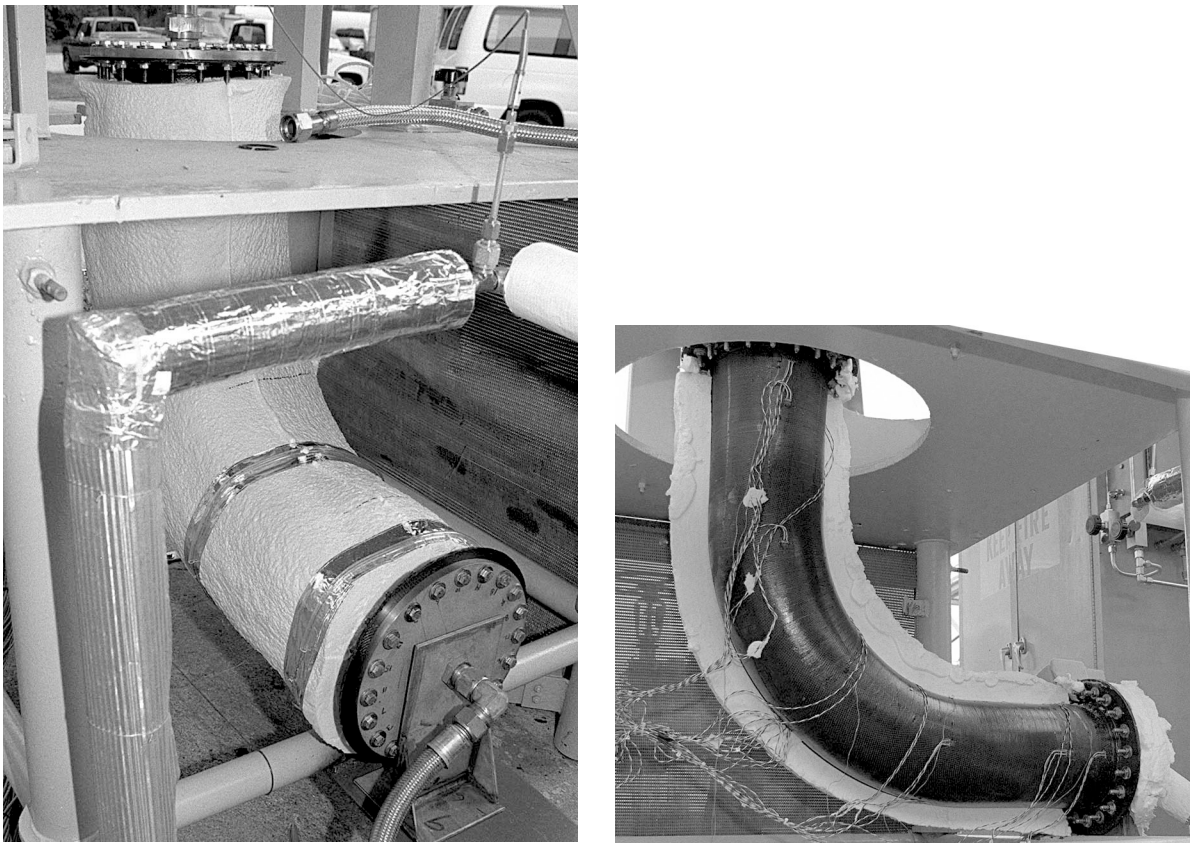

Figure 38. Test article HLU–2 in test stand 300. Shown with full insulation and half of the insulation removed.

4.3.1 Test Articles Manufactured via Hand Layup

The first feedline to undergo cryogenic testing was feedline HLU–2. It passed all the thermal and pressurization cycle testing. No leaks ever developed in this feedline. The pressure, temperature, and strain data are recorded and stored in a digital format for comparison to analysis. After the cryogenic testing of HLU–2 with LH_2, a posttest leak check was made. Using a GHe mass spectrometer, the leakage measured from the feedline was $\leq 2.0 \times 10^{-8}$ sccs GHe. This value was essentially the background He in the room where the measurement took place. The conclusion was the feedline was not leaking and passed its cryogenic tests.

The second feedline to undergo cryogenic testing was feedline HLU–7. It passed all the thermal and pressurization cycle testing. No leaks ever developed in this feedline. The pressure, temperature, and strain data are recorded and stored in a digital format for comparison to analysis. After the cryogenic testing of HLU–7 with LH_2, a posttest leak check was made. Using a GHe mass spectrometer, the leakage measured from the feedline was $\leq 1.4 \times 10^{8}$ sccs GHe. This value was essentially the background He in the room where the measurement took place. The conclusion was the feedline was not leaking and passed its cryogenic tests.

4.3.2 Test Articles Manufactured via Solvent-Assisted Resin Transfer Molding

SARTM–2 was the first feedline of this type to be tested. During the first cryogenic cool-down cycle with LN_2, strain gauge readings were being lost. Upon closer inspection, it was noted that LN_2 was pouring out from the insulation around the feedline. The insulation was removed and it appeared that the LN_2 was seeping out of the tube across its entire acreage. The cryogenic testing was stopped and a GHe leak check was performed. The feedline was filled with 10 psi of GHe and a leak detect solution was sprayed over the feedline. Leakage was observed over the entire area of the feedline. Figure 39 shows the extent of the leakage on this tube. Feedline SARTM–4 was then filled with LN_2 and yielded the same results as feedline SARTM–2. Cryogenic testing on these feedlines was terminated at this point.

Figure 39. Leakage across feedline SARTM–2 after first introduction of LN_2 into the feedline.

Feedline SARTM–2 was then dissected for inspection as to the mechanisms behind this gross leakage. Figure 40 shows a view of the inside surface of the tube after a UV dye was placed on the surface. For comparison, a SARTM tube that did not undergo cryogenic testing is also shown. Many matrix cracks can be seen on the specimen that saw one temperature drop to LN_2 temperature.

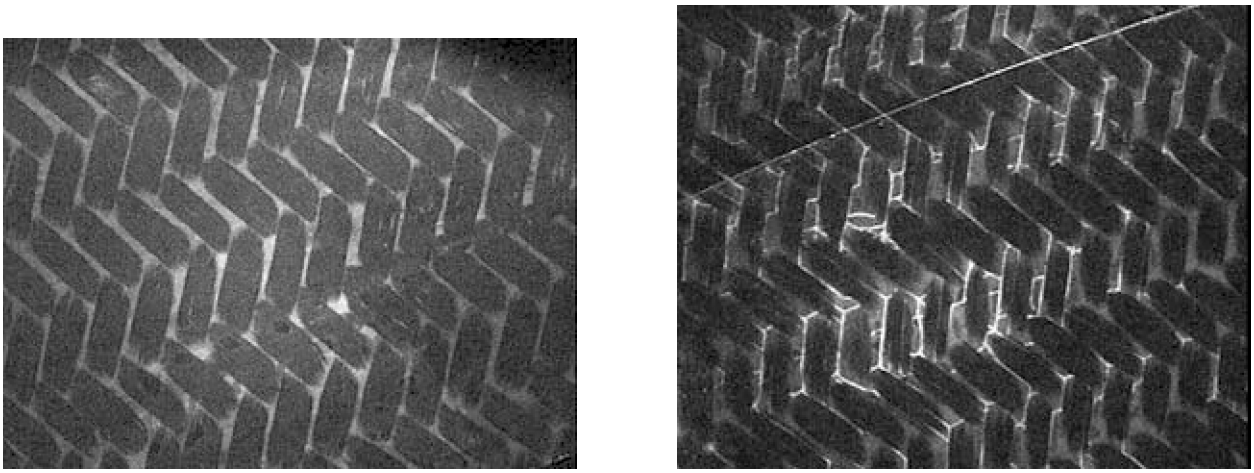

(a) (b)

Figure 40. Inside surface of SARTM feedlines: (a) No cryogenic temperature and (b) LN_2 temperature excursion.

Figure 41 is a view of the outside of a SARTM feedline that saw a temperature drop to LN_2. A section of a SARTM feedline that did not experience cryogenic temperatures is also shown for comparison.

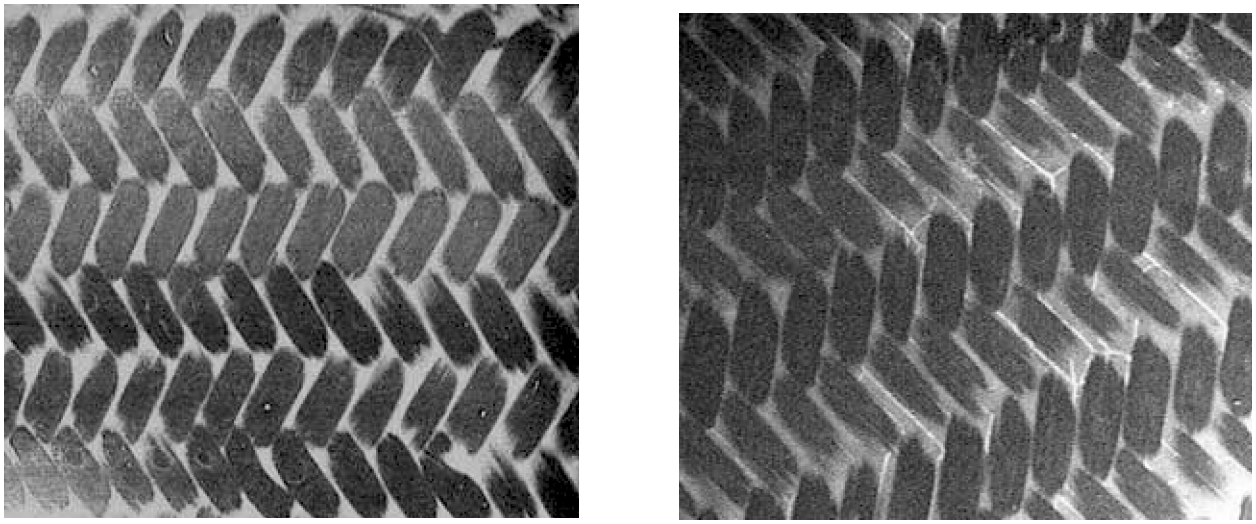

(a) (b)

Figure 41. Outside surface of SARTM feedlines: (a) No cryogenic temperature and (b) LN_2 temperature excursion.

4.4 Burst Pressure Testing

Feedline HLU–2 was hydrostatically tested for burst strength. The feedline was installed such that both flanged ends were rigidly fixed to prevent any movement. A maximum pressure of 545 psi was reached and then the feedline catastrophically failed. A photograph of the failed feedline is shown in figure 42. A longitudinal split is seen on most of the feedline with a radial split occurring about three quarters of the way up the tube.

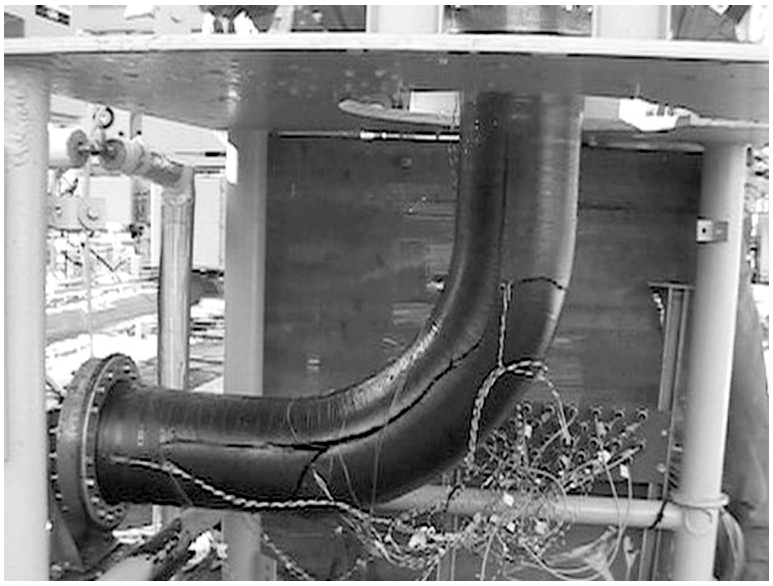

Figure 42. Feedline HLU–2 after failing at 545-psi internal pressure.

Feedline HLU–7 was then hydrostatically tested for burst strength. It was also installed such that both flanged ends were rigidly fixed to prevent any movement. A maximum pressure of 364 psi was reached and then the feedline catastrophically failed. Photographs of the failed feedline are shown in figure 43. A large split about one fourth of the tube length is seen along one side.

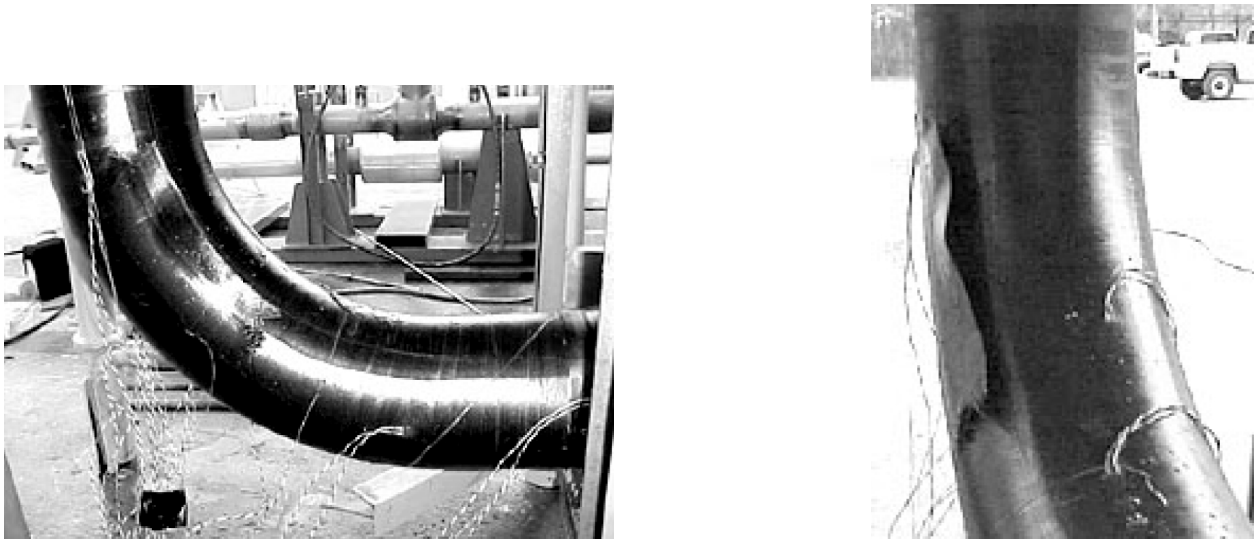

(a) (b)

Figure 43. Feedline HLU–7 after failing at 364-psi internal pressure.

4.5 Damage Tolerance Testing

One of the critical technology drivers for composite components is resistance to foreign object impact damage. This is especially important in applications in which leak paths must not develop in a component such as a feedline. The materials examined all have a five-harness weave of IM7 as the fiber constituent (except for the thermoplastic, which is unidirectional tape laidup in a bidirectional configuration). The resins tested were RS–E3 (electron-beam curable), PEEK (thermoplastic), 977–6, Cycom 823, PR 520, and SE–SA–1 (all epoxies). Since a limited amount of material was available for impact testing, relatively small specimens were used. This was not a problem since the actual feedline would experience mostly contact force damage rather than damage due to large deformation. This is based on a previous study on impact damage to composite feedlines which found that through the thickness leak paths developed as a result of contact force damage.[2] Impact damage resistance will be one of the critical parameters when choosing a fiber/resin system since one of the main goals of future space vehicles is increased reliability.

It would be desirable to use these feedlines without liners that add complexity and weight to the hardware. This makes permeation after impact testing critical to the success of the program. This type of testing is new and has not been as extensively studied as compression after impact. Studies that have been performed in this area mostly pertain to using liners in composite fuel tanks.[3,4] The helicopter industry has been concerned about water ingression in honeycomb structures and has studied water permeation after impact.[5] The results indicate that a liner is needed for thin face sheets. However, none of these studies examined the harsh thermal environment of cryogenic composite structures, nor do they address gas permeation through a laminate due to microcracking. Gas permeation through composites has been studied in the rocket nozzle industry since an ablative's performance is related to its permeability,[6] but this does not concern impact damage to the composite.

It is the intent of this study to gain insight into the relative resistance to microcracking due to an impact event of some candidate resins being examined for use on feedlines.

4.5.1 Material Used

There were six material systems tested in this study. These, along with some of their laminate properties, are presented in table 2.

Table 2. Materials tested for impact resistance.

Material System[1]	Manufacturing Method	Type Resin	Laminate Density (g/cm^3)	Laminate Modulus (Msi)	Laminate Tensile Strength[3] (ksi)	Laminate Compression Strength[4] (ksi)
IM7/977–6	HLU with autoclave cure	Toughened Epoxy	1.35	10.2	130.0	83.9
IM7/PR 520	SARTM[2] with autoclave cure	Toughened Epoxy	1.58	10.2	124.8	73.1
IM7/Cycom 823	SARTM with autoclave cure	Toughened Epoxy	1.63	10.2	120.0	63.1
IM7/SI–SE–1	SARTM with autoclave cure	Epoxy	1.55	10.2	115.0	54.2
IM7/RS–E3	HLU with electron beam cure	Epoxy	1.55	10.2	120.0	80.1
IM7/PEEK	HLU with hot press cure	Polyetheretherketone	1.59	11.5	160.0	68.6

[1] All laminates made from five-harness woven fabric $[0/90]_{2S}$ (except IM7/PEEK which is made from unitape $[0,90,0,90]_S$).

[2] SARTM

[3] ASTM D 3039

[4] ASTM D 3410M

All of the panels were visually inspected before test coupons were cut from them. Areas of the panels had their cross sections examined as part of another test series and no panels contained voids of any significance and all were well consolidated. Since material was limited, small impact specimens were chosen for testing. These specimens were squares 2.25 in. on a side.

4.5.2 Impact Testing

A drop-weight impact test apparatus was used for the testing. The square specimens were supported over a 2×2-in. square opening and impacted at the center with a 0.25-in. instrumented tup (striker). A few sacrificial specimens were impacted and an impact level was chosen that would produce obvious damage in most of the materials tested. This turned out to be a weight of 2.5 lbf dropped from a height of 12 in. for an impact energy of 2.5 ft-lb. This was considered the upper threshold of the impact severity and subsequent impact testing would be conducted at a level that would cause less damage. Load-time data were gathered by a GRC 930–I software system for later reduction if desired. Each type of material system was impacted twice at each of the two energy levels tested to ensure repeatability. In all cases, the impacts were nearly identical in every way so repeatability was not a concern.

An impact energy level of 1.8 ft-lb was also used to observe the damage resistance of these materials at a lower severity of impact. The two impact levels used will often be referred to as high (2.5 ft-lb) and low (1.8 ft-lb) throughout this TP.

The damage resistance was evaluated in three ways: (1) Visual examination, (2) radiography, and (3) cross-sectional examination.

4.5.3 Visual Examination

After each impact event, the specimen surface damage was recorded as a digital image. Both sides of the specimen were observed and recorded.

4.5.4 Radiography

Each impacted specimen was subjected to a dye penetrant soak for at least 24 hr. The dye penetrant was a zinc iodide (ZnI_2) solution containing Kodak PhotoFlo™ to help the penetrant flow into all cracks and delaminations that may have been formed. The ZnI_2 solution is opaque to x rays and shows when an x-ray image of the specimen is made, thus forming a map of the damage within the specimen. This technique was only used on specimens impacted at the high energy level (2.5 ft-lb) since the next energy level used (1.8 ft-lb) did not produce enough damage to be readily seen on an x ray.

4.5.5 Cross-Sectional Examination

After the specimens were x-rayed, they were sectioned through the center of the impact area with a diamond-wafering blade. The halved specimens were then mounted in polymethylmethacralate for subsequent edge polishing and microscopic examination. The specimens were sectioned parallel to the warp fibers on the outer surfaces of the specimens, or parallel to the outer 0° fibers on the IM7/PEEK specimens. The edges were wet polished with silicon-carbide paper of progressively finer grit sizes: 240, 400, 600, 800, 1,000, and 1,200. A fluorescent dye was placed on the polished edges of the specimen and wiped off so that the dye remained in any cracks in the specimen. Upon exposure to a UV light source, any damage present would then be highlighted and much easier to detect.

4.5.6 Visual Examination After Impact (High-Level Impacts)

Figure 44 shows the impacted side of each specimen tested at the high (2.5 ft-lb) energy level. In all cases, except the 977–6 resin, a distinct dent is seen in each of the specimens. Fiber breakage is observed in all of the specimens. The 977–6 resin possesses a relatively long crack across the outer warp fibers that span the distance of the impacted zone. The PR 520 has short cracks at or near the indentation formed, as does the PEEK. The remaining three have fiber breakage within the indentation.

Figure 45 shows the back (nonimpacted) side of each type of specimen tested at the high (2.5 ft-lb) energy level. All samples show backface fiber breakage of varying magnitudes. The 977–2 is the least severe while the RS–E3 and Cycom 823 are the most severe where it appears near penetration occurred.

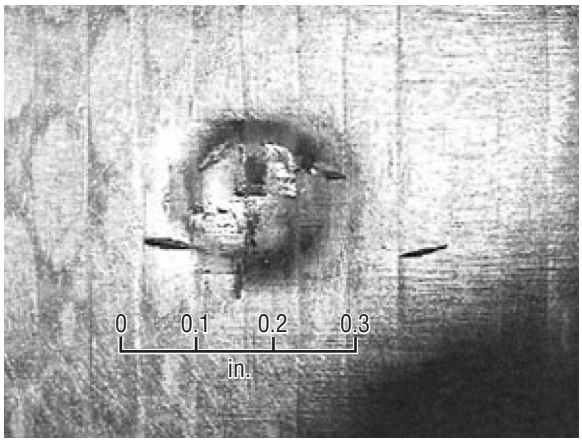

IM7/PR 520

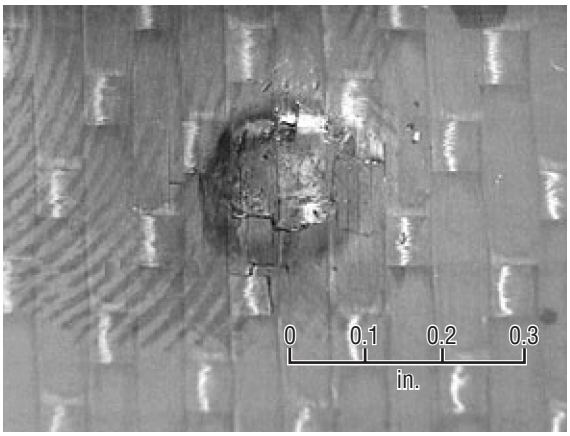

IM7/SI–SE–1

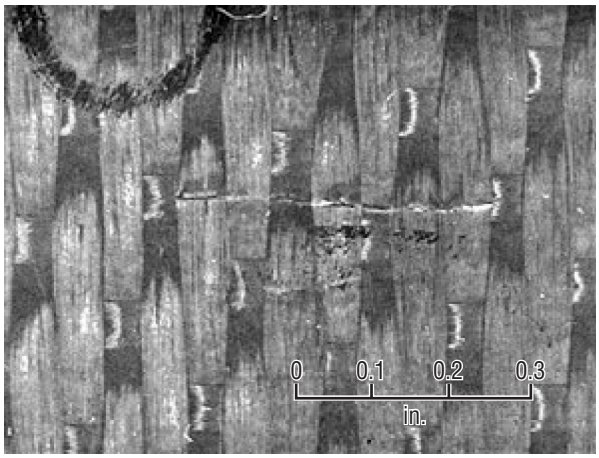

IM7/977–6

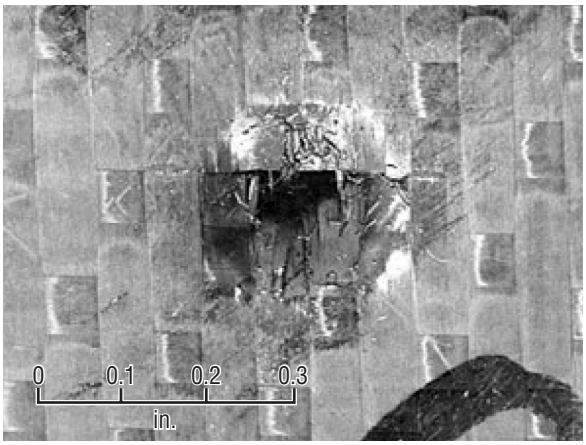

IM7/Cycom 823

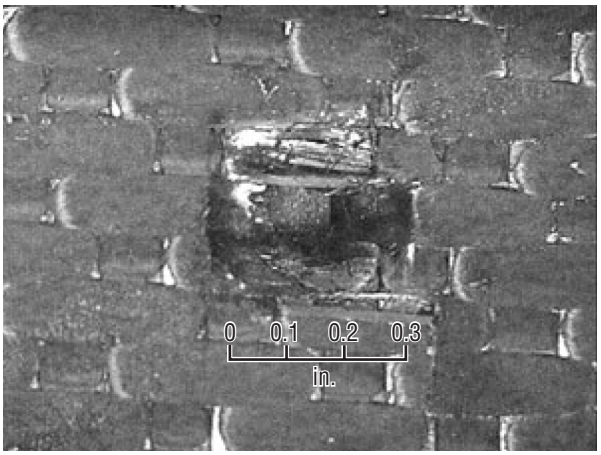

IM7/RS–E3

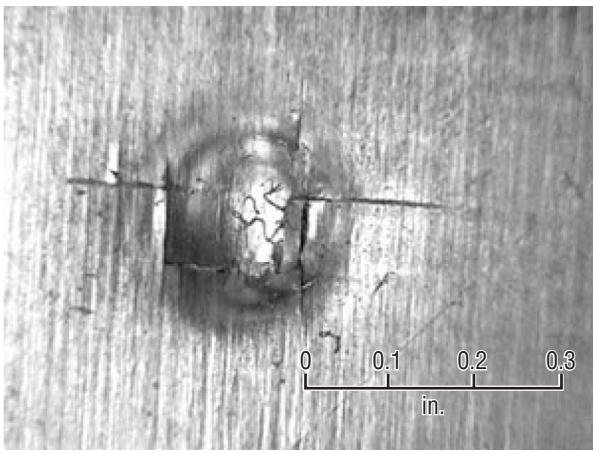

IM7/PEEK

Figure 44. Typical damage to impacted side of specimens at 2.5 ft-lb.

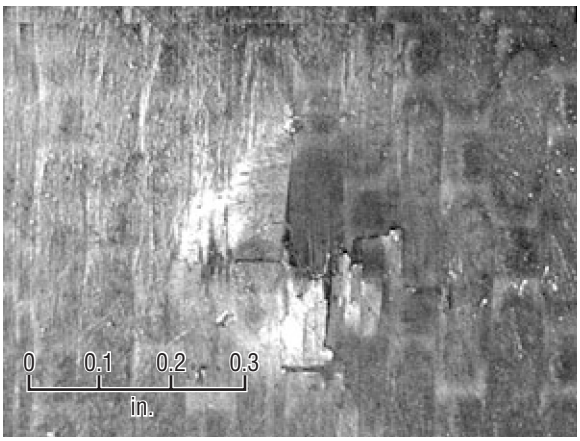

IM7/PR 520

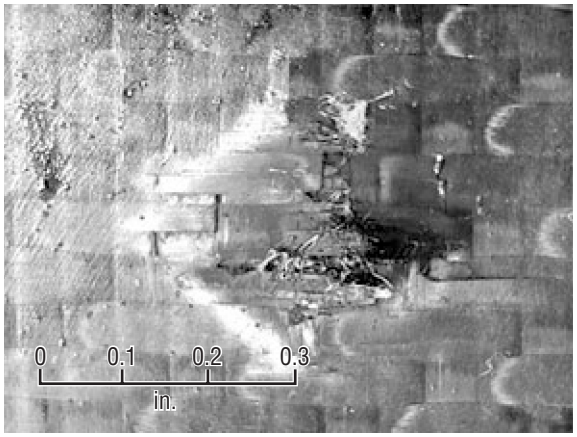

IM7/SI–SE–1

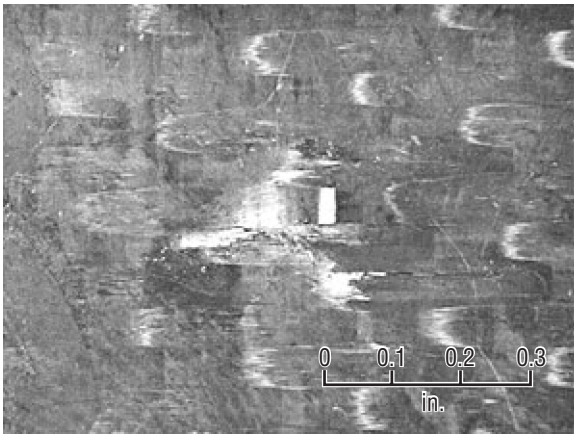

IM7/977–6

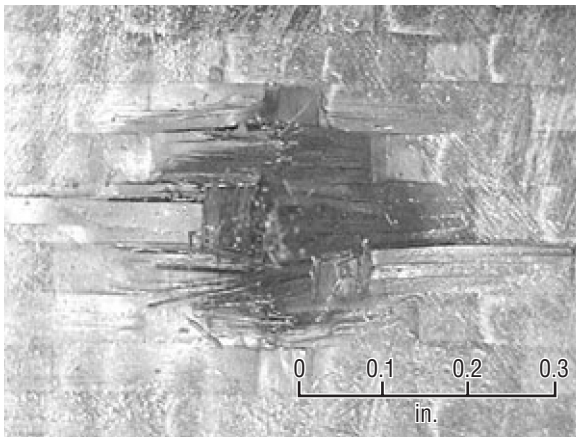

IM7/Cycom 823

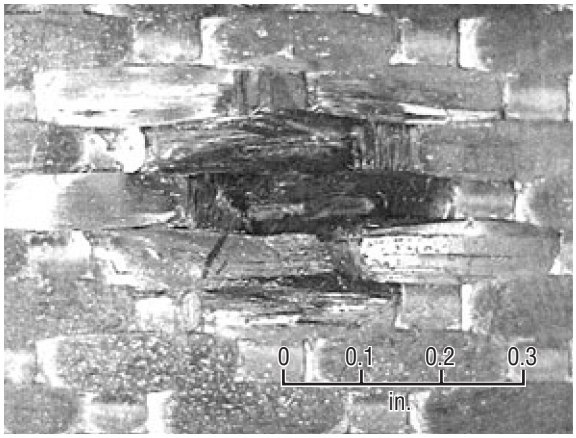

IM7/RS–E3

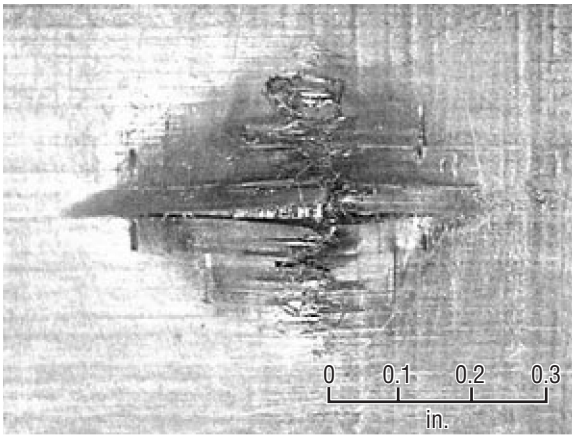

IM7/PEEK

Figure 45. Typical damage to nonimpacted side of specimens at 2.5 ft-lb.

4.5.7 Radiography After Impact (High-Level Impacts)

Figure 46 shows x rays of each type of resin system tested at the high-impact energy level. These x rays correspond to the visual observations of figures 44 and 45. The 977–6-resin system has noticeably less damage than the others. The Cycom 823 and RS–E3 systems appear as dark circles indicating massive damage directly under the impact zone. Delaminations emanating from the impact can be seen in the Cycom 823, RS–E3, and PEEK resin systems.

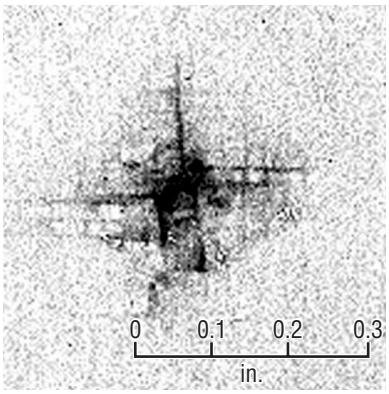

IM7/PR 520

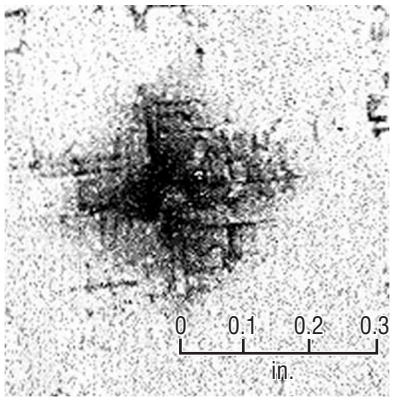

IM7/SI–SE–1

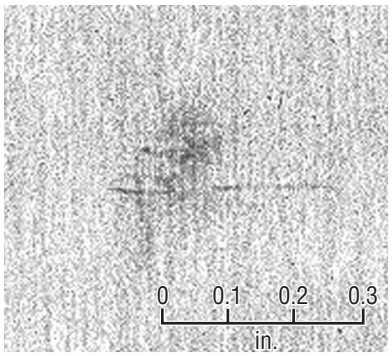

IM7/977–6

IM7/Cycom 823

Figure 46. X rays of specimens impacted at 2.5 ft-lb.

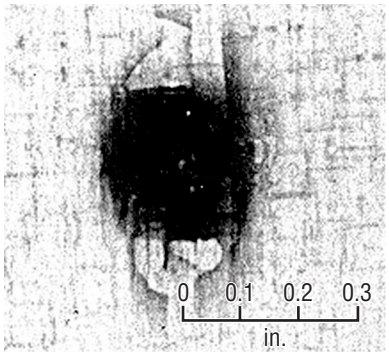

IM7/977–6

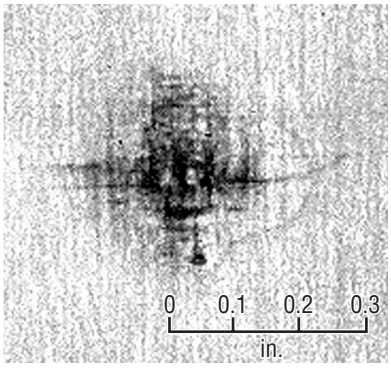

IM7/PEEK

Figure 46. X rays of specimens impacted at 2.5 ft-lb (continued).

4.5.8 Cross-Sectional Examination (High-Level Impacts)

Figures 47 show photomicrographs of the cross section of each type of resin system tested at the high-impact energy level. The 977–6 and PEEK resins appear to have far less damage than the others tested. The Cycom 823 and RS–E3 resins show near penetration.

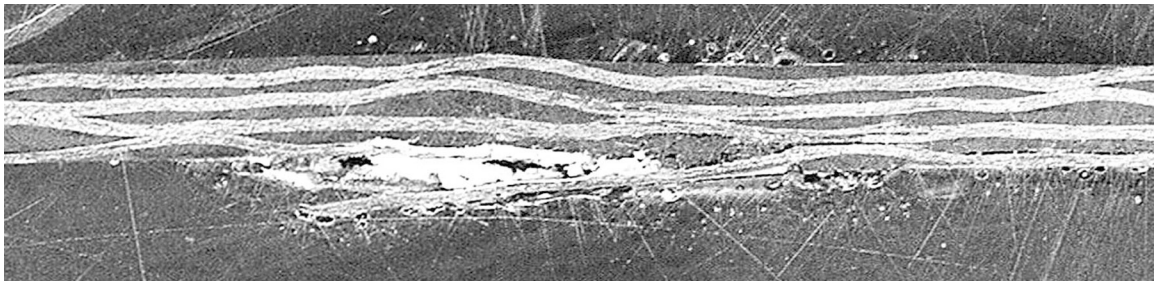

IM7/PR 520

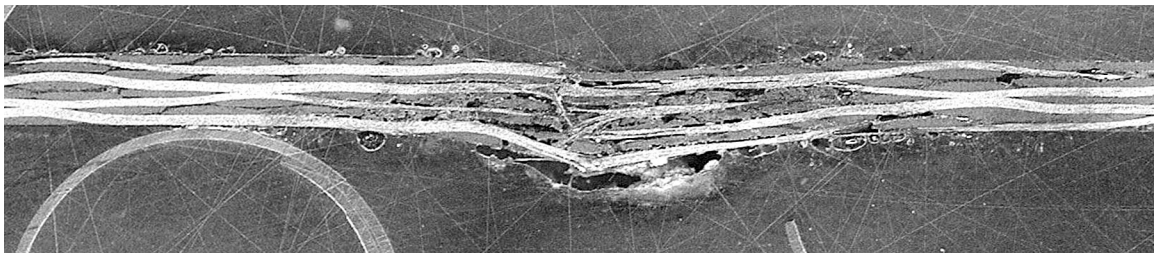

IM7/SE–SE–1

Figure 47. Cross-sectional photomicrographs of specimens impacted at 2.5 ft-lb.

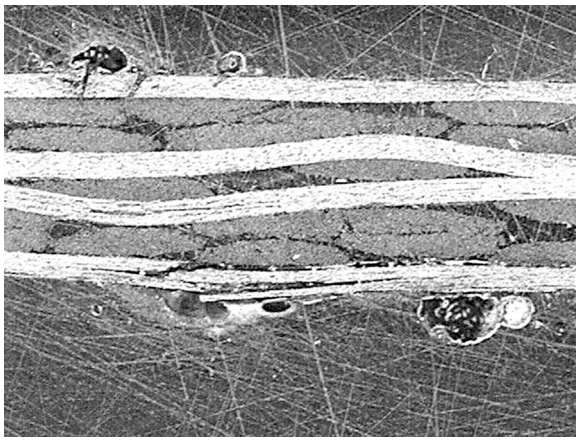

IM7/S977–6

IM7/Cycom 823

IM7/RS–E3

Figure 47. Cross-sectional photomicrographs of specimens impacted at 2.5 ft-lb (continued).

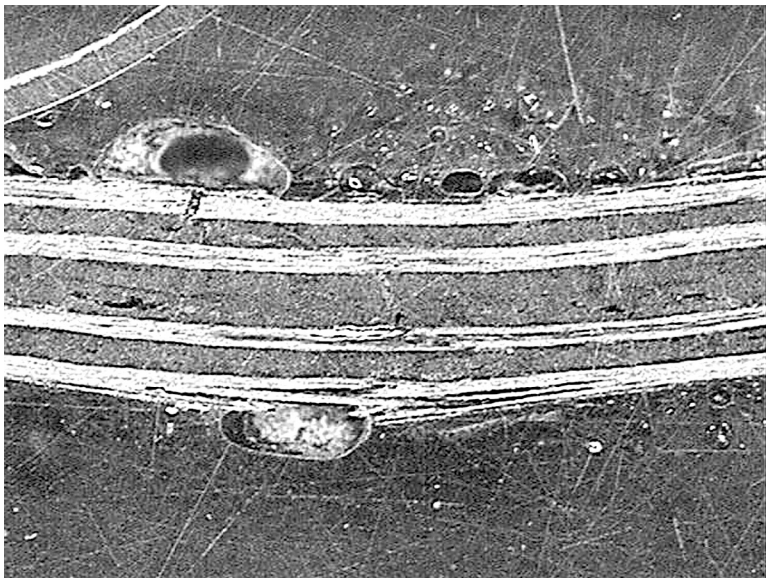

IM7/PEEK

Figure 47. Cross-sectional photomicrographs of specimens impacted at 2.5 ft-lb (continued).

Figures 48 show fluorescent dye-enhanced photographs of these cross sections. This technique better shows the extent of damage present in the specimens. The 977–6 specimen only has two short delaminations near the outer plies and minor fiber breakage on the top ply. The plies in the center of the specimen appear to be completely damage free. The PEEK specimen shows good damage resistance; however, damage does exist throughout the thickness of the specimen. The severity of damage to the Cycom 823 and RS–E3 resin systems are even further highlighted by the fluorescent dye. The PR 520 resin system is seen to have delamination and matrix cracking within all plies although the photograph in figure 47 does not clearly show this and is a good argument for using a fluorescent dye penetrant even on samples where damage is readily visible.

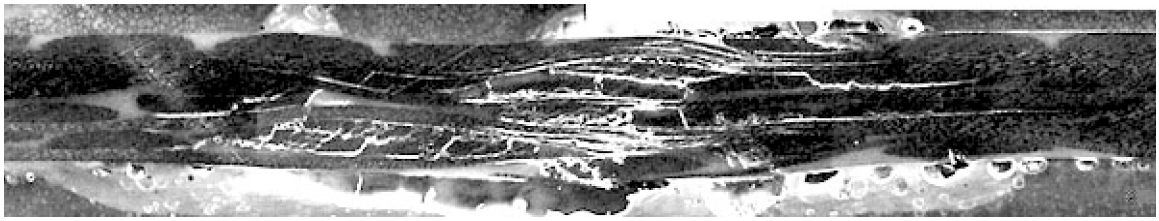

IM7/PR 520

Figure 48. Cross-sectional photomicrographs of specimens impacted at 2.5 ft-lb, fluorescent dye enhanced.

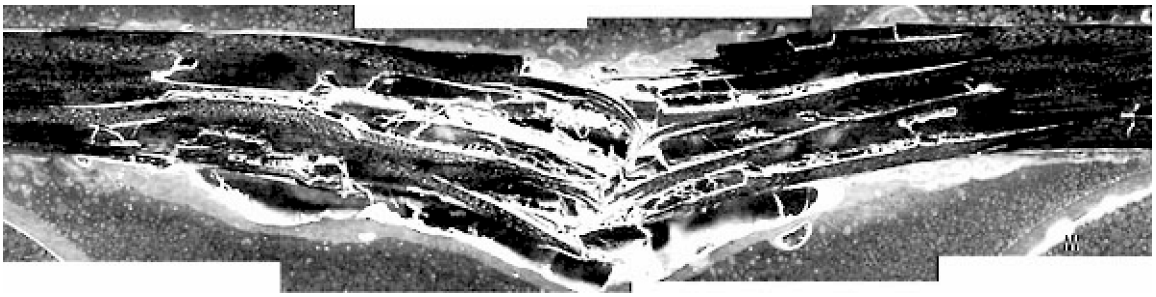

IM7/SI–SE–1

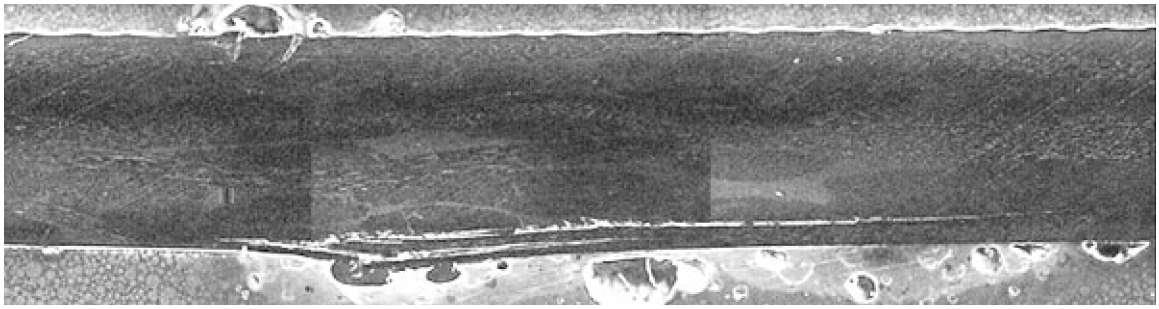

IM7/977–6

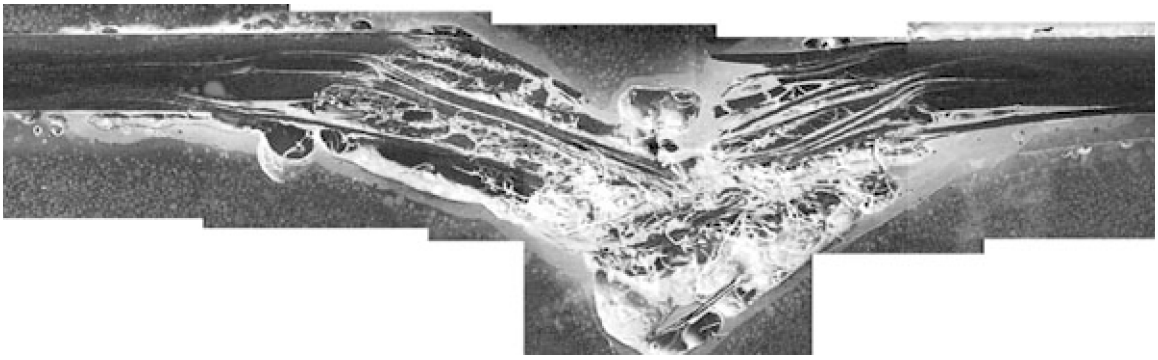

IM7/Cycom 823

IM7/RS–E3

Figure 48. Cross-sectional photomicrographs of specimens impacted at 2.5 ft-lb, fluorescent dye enhanced (continued).

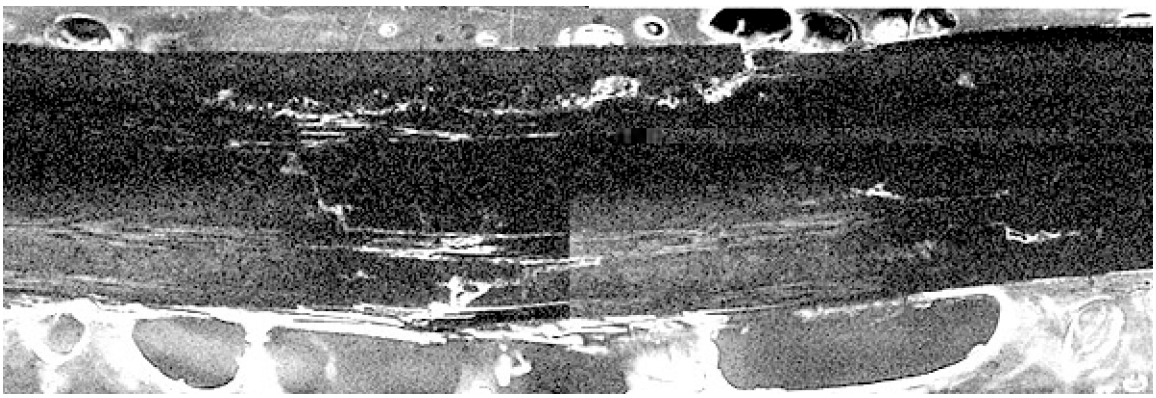

IM7/PEEK

Figure 48. Cross-sectional photomicrographs of specimens impacted at 2.5 ft-lb, fluorescent dye enhanced (continued).

4.5.9 Visual Examination After Impact (Low-Level Impacts)

Figure 49 shows the impacted side of each specimen tested at the low (1.8 ft-lb) energy level. Fiber breakage is observed in most of the specimens in the form of short cracks emanating from the indentation on the surface. The RS–E3 resin has a long, fine crack that runs from the lower left to the upper right of the figure and very little indentation is observed. The mechanics behind these small cracks is unknown, but they have been noted in a previous study.[7]

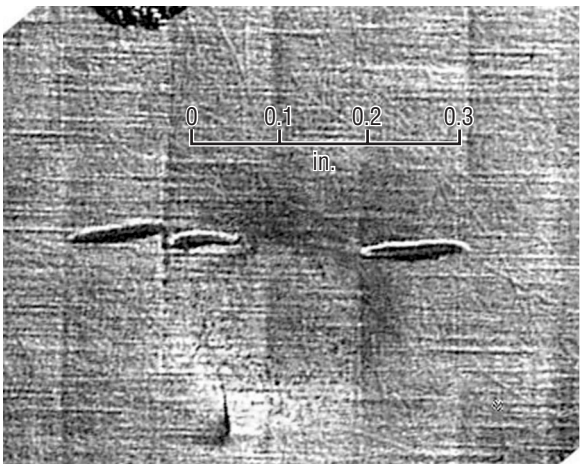

IM7/PR 520

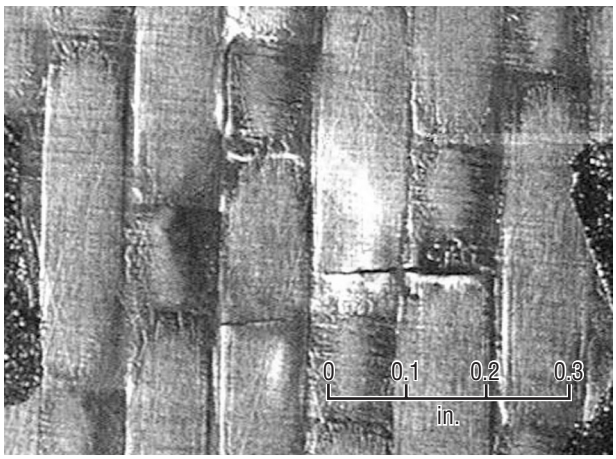

IM7/SI–SE–1

Figure 49. Typical damage to impacted side of specimens at 1.8 ft-lb.

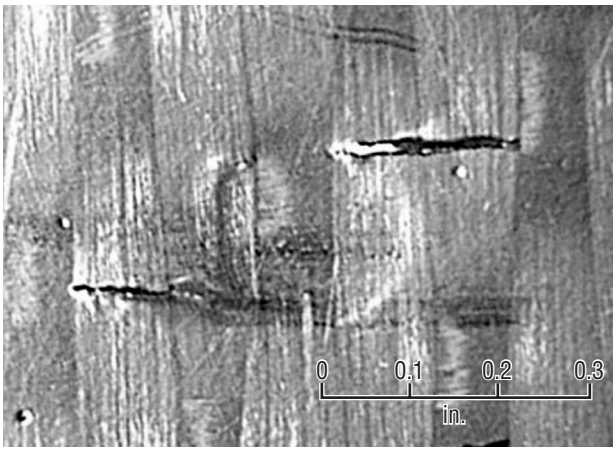

IM7/977–6

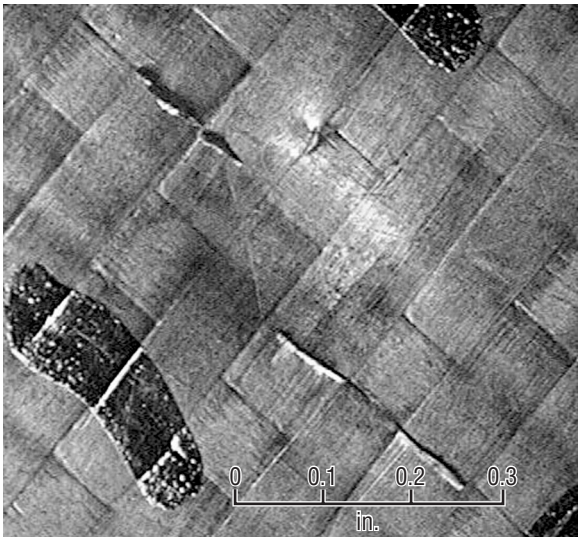

IM7/Cycom 823

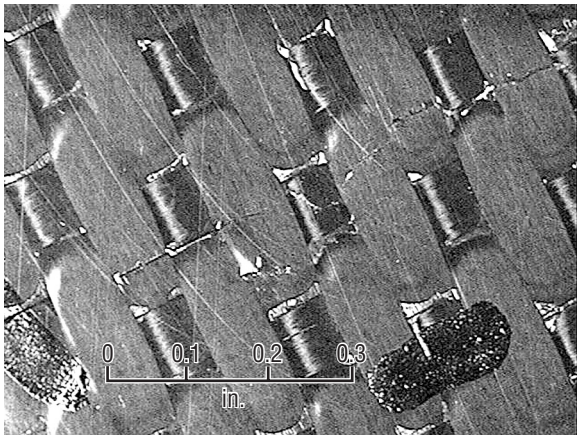

IM7/RS–3

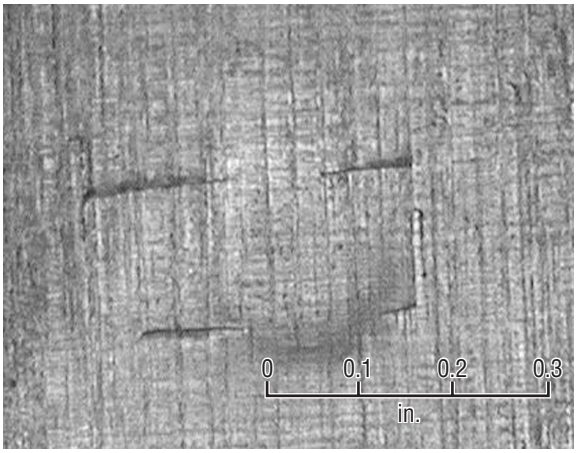

IM7/PEEK

Figure 49. Typical damage to impacted side of specimens at 1.8 ft-lb (continued).

Figure 50 shows the back (nonimpacted) side of each type of specimen tested at the low (1.8 ft-lb) energy level. All samples show backface fiber breakage of varying magnitudes. The 977–6 and RS–E3 resin systems have barely noticeable backface damage. What little damage is present in these two systems is limited to less than two stitches, but never three or more. This type of damage could easily be overlooked during a routine inspection of a part.

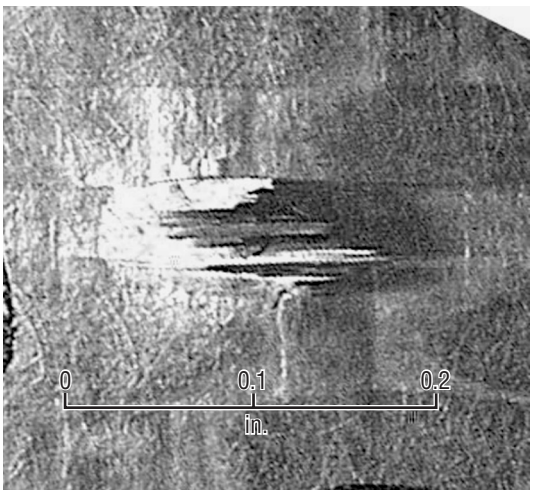

IM7/PR 520

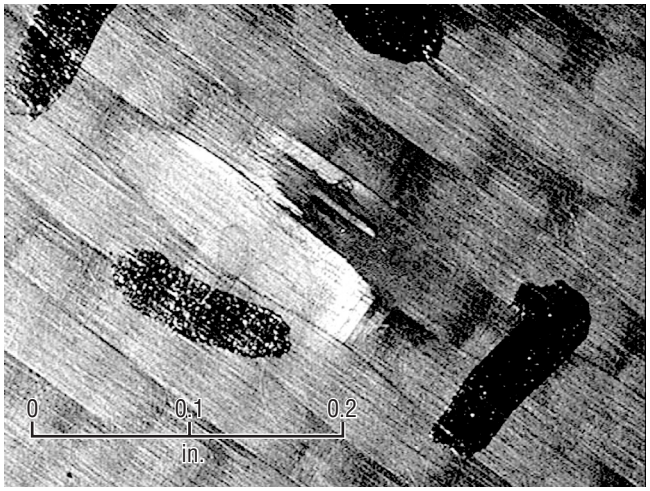

IM7/SI–SE–1

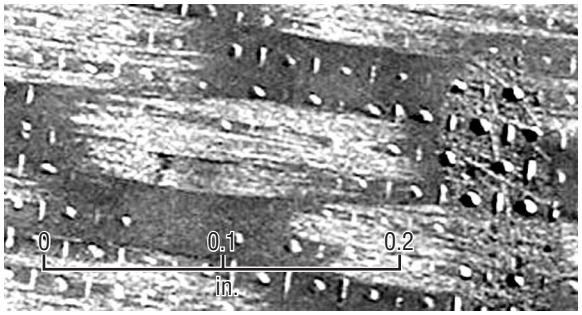

IM7/977–6

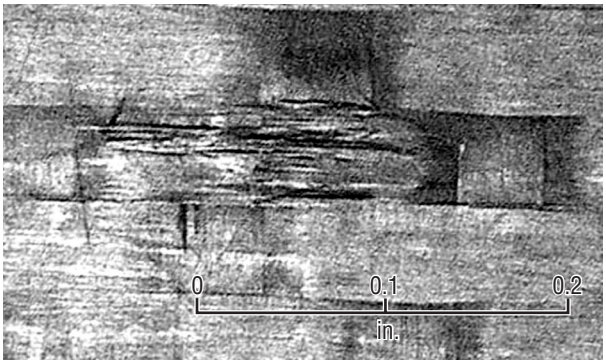

IM7/Cycom 823

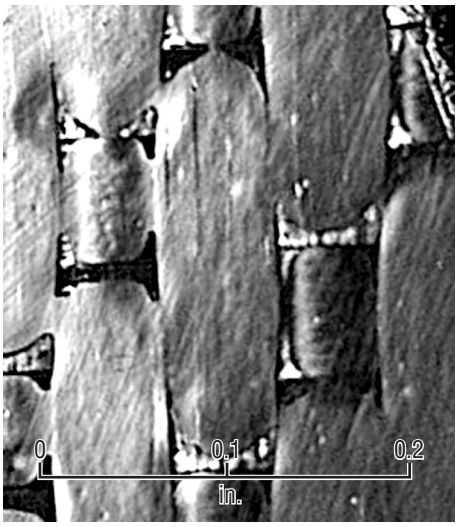

IM7/RS–E3

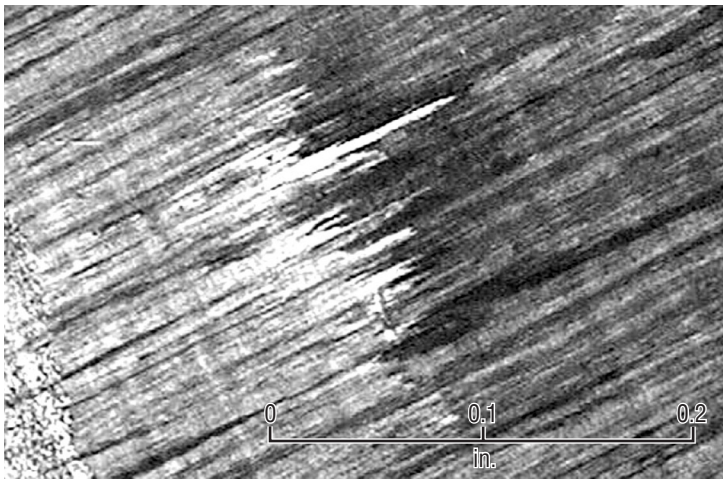

IM7/PEEK

Figure 50. Typical damage to nonimpacted side of specimens at 1.8 ft-lb.

4.5.10 Radiography After Impact (Low-Level Impacts)

No radiographs were taken of these specimens since such little damage was formed and an x-ray signature of the damage would yield no information.

4.5.11 Cross-Sectional Examination After Impact (Low-Level Impacts)

Figure 51 shows photomicrographs of the cross section of each type of resin system tested at the low-impact energy level. The fluorescent dye technique was employed on all of these specimens since visible light did not readily detect all of the damage present. The 977–6 and the PEEK resins showed the least amount of damage, as they did for the high-impact energy level. The 977–6 resin showed a short delamination at the bottom plies and some matrix cracking within the bottom ply, but the majority of the cross section is undamaged. The PEEK resin showed similar damage with some small delaminations and matrix cracking in or near the bottom ply.

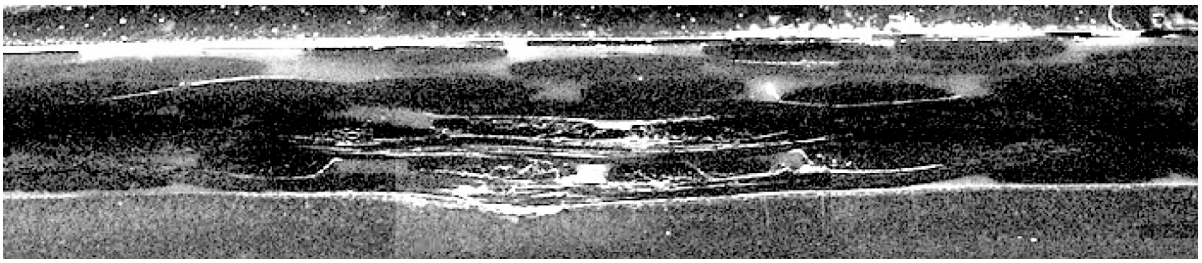

IM7/PR 520

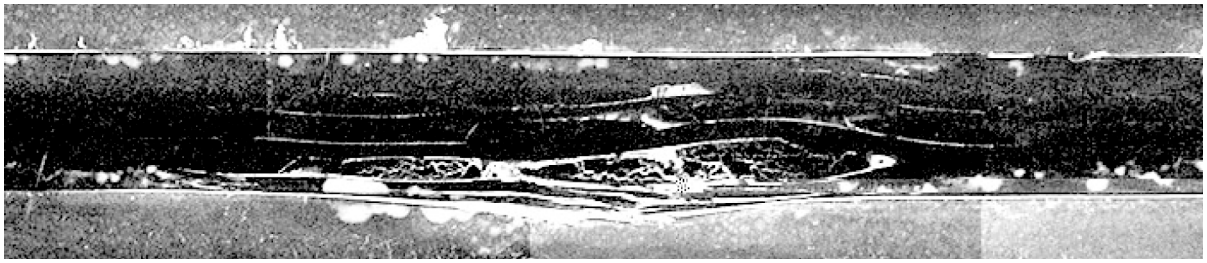

IM7/SE–SE–1

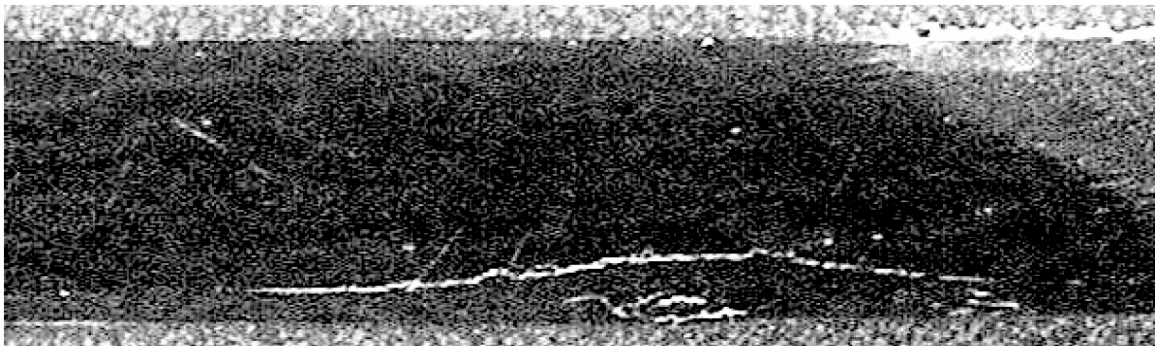

IM7/977–6

Figure 51. Cross-sectional photomicrographs of specimens impacted at 1.8 ft-lb.

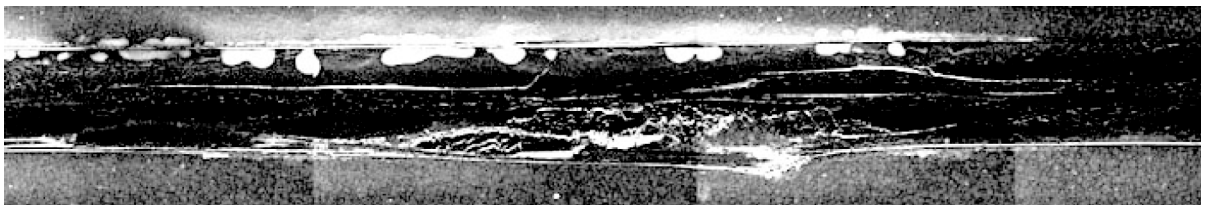

IM7/Cycom 823

Far View

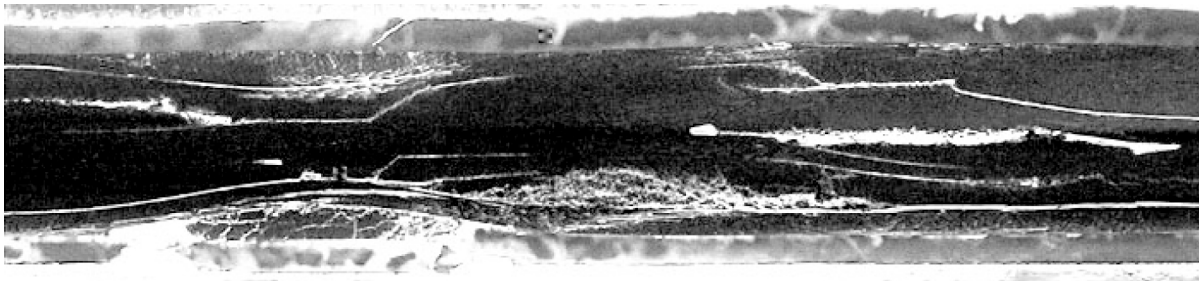

Close View

IM7/RS–E3

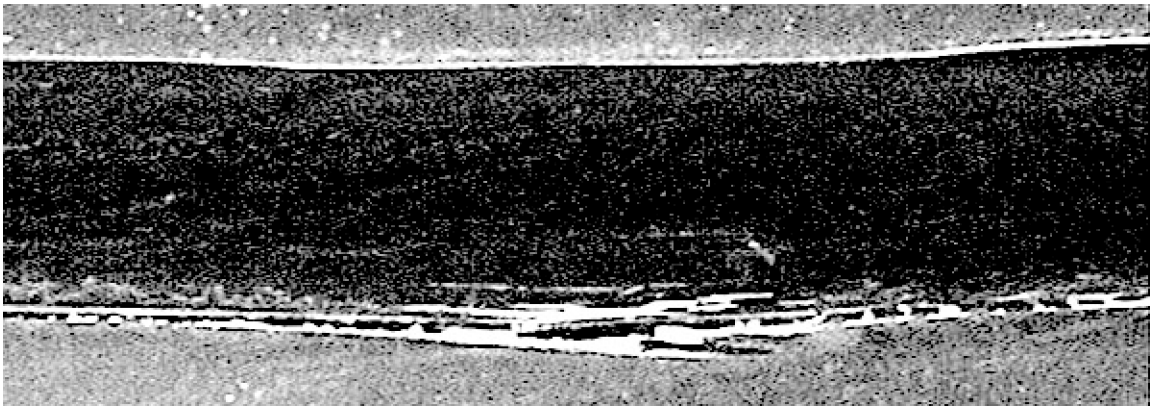

IM7/RS–E3

Figure 51. Cross-sectional photomicrographs of specimens impacted at 1.8 ft-lb (continued).

The RS–E3 resin system had extremely long delaminations emanating from the impact damage, so two pictures are presented to include the entire range of damage.

4.5.12 Conclusions of the Damage Tolerance Study

From the results in this study, it appears that the 977–6 resin system is far superior to the others tested for microcracking resistance to impact damage. The PEEK resin system also demonstrated good impact resistance. The Cycom 823 and RS–E3 demonstrated poor impact resistance as many delaminations and microcracks were found in these specimens at the low-impact energy level.

The use of a fluorescent dye to highlight damage gives a better indication of damage when examining the cross section of an impacted specimen.

4.6 Permeability After Impact Testing

As composite laminates are being considered for use in liquid propulsion systems, microcracking due to foreign object impact damage becomes very important, especially if a tank or feedline is to be unlined. If a component that carries liquid or gaseous hydrogen develops an area of microcracking, hydrogen can leak out of the component and pose a serious threat to the vehicle. Since it has been shown in the past that no visible impact damage can cause a composite feedline to leak,[2] a better understanding of the material's resistance to microcracking is needed. Microcracking also occurs due to thermal and mechanical stresses and fatigue; however, this study will deal only with foreign object impact damage, a very real threat to all composite parts. The most quantifiable way of determining how much leakage may occur after an impact event is to test the material for permeability. Permeability testing has been used in the past for composites to determine the porosity of rocket nozzle material.[6] Fluid permeability has been tested on some composite structures to be used as fuel tanks.[3,8] ASTM standard D 1434 exists for gas permeability testing of plastic film and sheeting and it is from this test methodology that the one in this study was adapted.

For this study, flat panel specimens were manufactured from material that was used in this feedline program. These specimens were representative of two of the carbon/polymer systems being evaluated for use in constructing feedlines for future launch vehicles. These were panels manufactured via HLU and electron beam curing. There was not enough material left to perform permeability tests on impacted specimens manufactured via SARTM or TTL. A drop-weight impact tester with a 0.25-in. diameter tup was used to impart varying levels of damage from almost nondetectable to near penetration. The specimens were then secured in a fixture that could supply a positive pressure of GHe on one side and allow a leak detection solution to be applied to the other side. This gave a qualitative assessment of permeability after impact. The specimens were then secured in an apparatus that could give quantitative results.

4.6.1 Experimental Procedure

This section will explain how the impact and subsequent permeability testing was performed. Results will be given in section 4.6.2.

4.6.1.1 Specimens. The HLU specimens were manufactured from carbon/epoxy prepreg that was in a five-harness satin weave form. A 36×24-in. panel was laidup in a bidirectional configuration on a flat aluminum tool. This gave the laminate a layup sequence of $[0/90,0/90]_S$. The panel was then vacuum

bagged and autoclave cured according to the manufacturer's recommended cure cycle. The electron beam laminates were manufactured in the same manner, only instead of an autoclave cure, electron beam radiation was used to cure the laminates. The cured laminates were then cut into 3×3-in. specimens. The nominal thickness of the specimens was 10 mil.

4.6.1.2 Impact Testing. The 3-in.-square specimens were impacted at various levels using a drop-weight apparatus. The impactor consisted of a 0.25 in. semispherically ended tup that was attached to a dynamic load cell to gather instrumented impact data, should it be needed for future analysis. (None of the instrumented data were used in the study presented in this paper). The falling mass had a total weight of 2.51 lb and drop heights of 4, 6, 8, 10, and 12 in. were used. The specimen was simply supported over a 2-in.-square opening. A schematic of the impact set up is given in figure 52. Two specimens were impacted from each drop height to give 10 impacted specimens in order to check for repeatability of results. After each specimen was impacted, images of both the front and back surface damage were recorded with a digital camera at a magnification of approximately × 5.

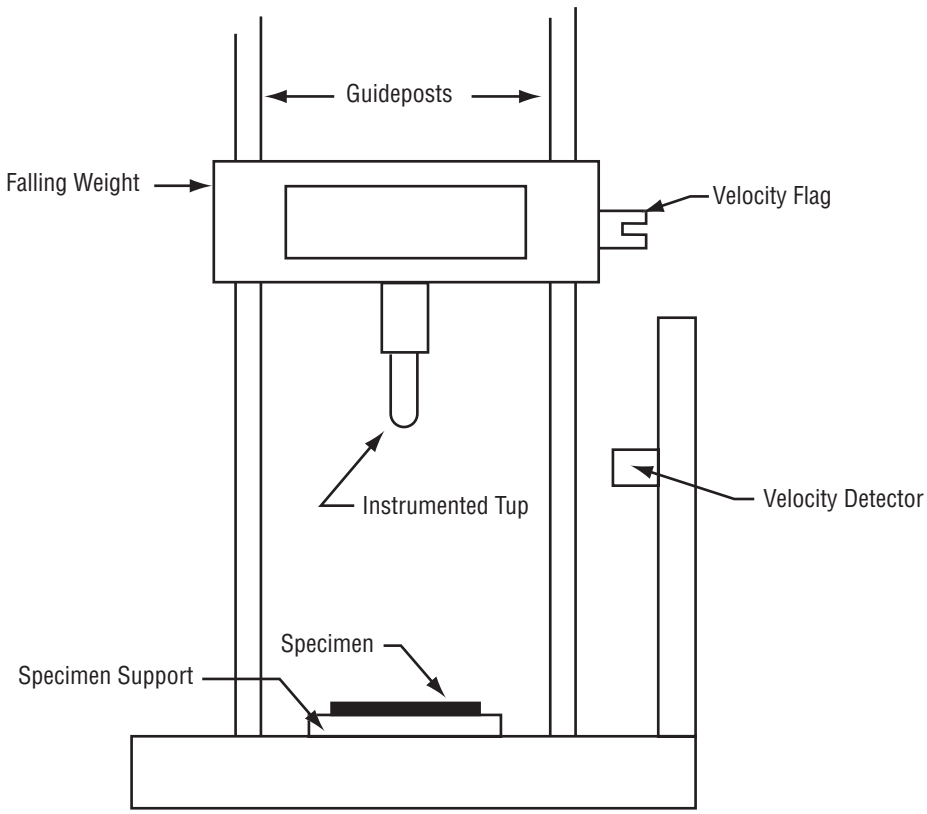

Figure 52. Schematic of impact apparatus.

4.6.1.3 Leak Check. After all specimens had been impacted and the surface damage recorded, the specimens were mounted in an apparatus to check for leakage of GHe when a positive pressure was applied to one side. A "bubble-type" leak detector solution was used and a digital image was made of the leaks for each specimen. A schematic of the apparatus used to check for leaks is shown in figure 53. A sample image of a leak is given in figure 54.

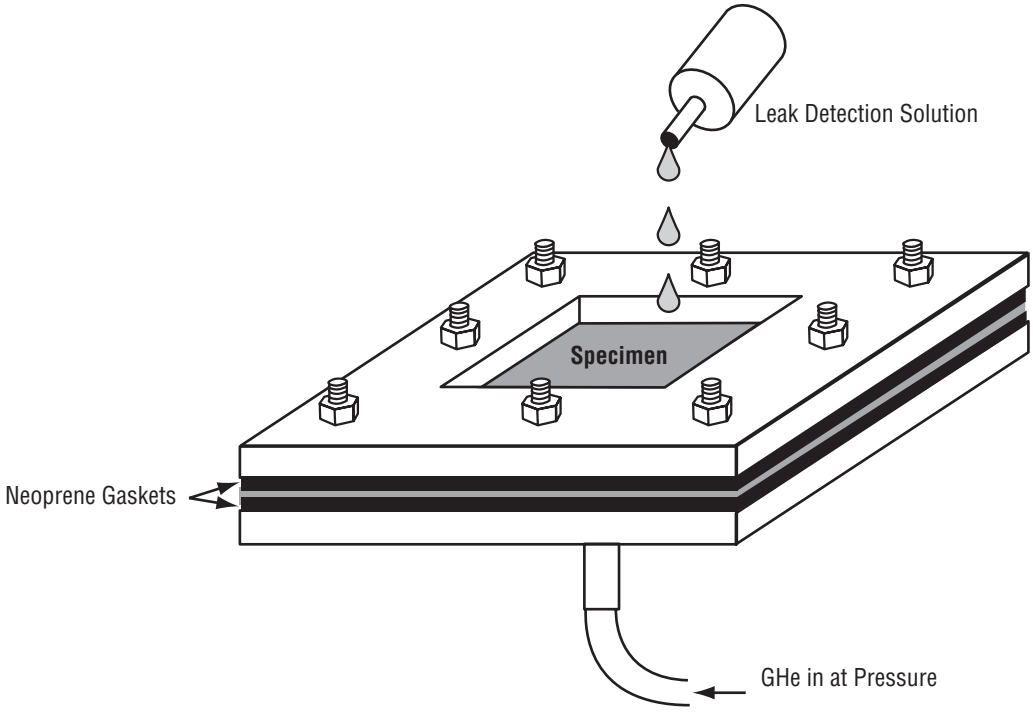

Figure 53. Schematic of leak detection apparatus.

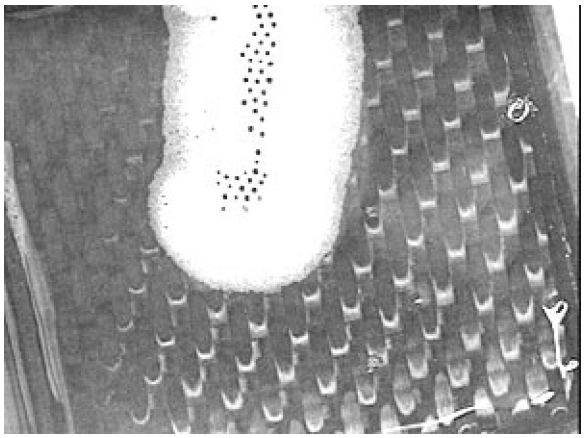

Figure 54. Specimen displaying a leak using a bubble-type leak detection fluid.

4.6.1.4 Permeability Testing. After the specimens had thoroughly dried from the leak detection procedure, they were ready for permeability testing. A more detailed analysis of the permeability testing and apparatus can be found elsewhere.[9]

4.6.2 Results

This section presents results of the impact testing, the leak check testing, and the permeability testing.

4.6.2.1 Impact Testing of Hand Layup Specimens. Ten specimens manufactured via HLU were impacted, two at each of the five energy levels. The resulting visual surface damage is presented in figure 55. Duplicates are not presented since the visual damage was nearly identical in every case. Damage in some form can be noted on all specimens, even those impacted at the smallest impact energy of 0.84 ft-lb.

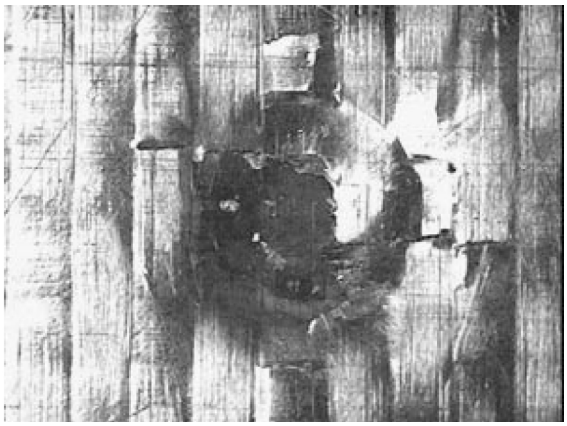

Front, Specimen 2, 2.51 ft-lb

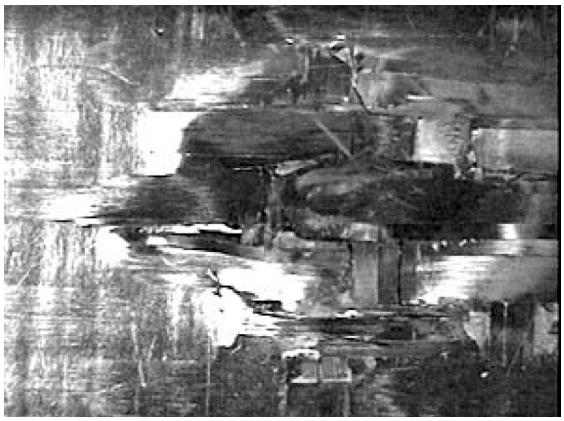

Back, Specimen 2, 2.51 ft-lb

Front, Specimen 3, 2.09 ft-lb

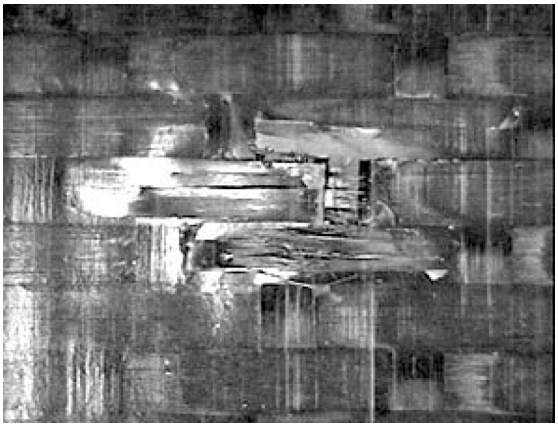

Back, Specimen 3, 2.09 ft-lb

Figure 55. Surface views of impacted HLU specimens.

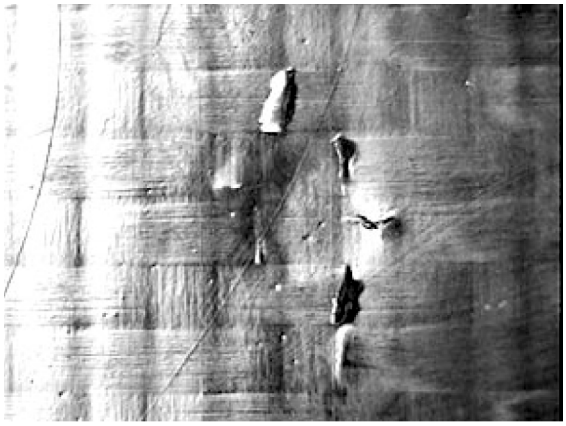

Front, Specimen 4, 1.67 ft-lb

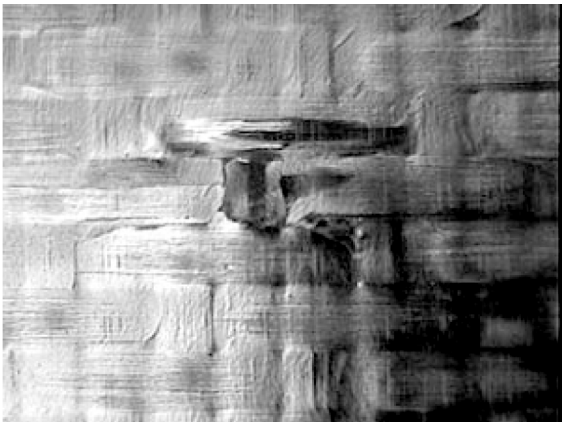

Back, Specimen 4, 1.67 ft-lb

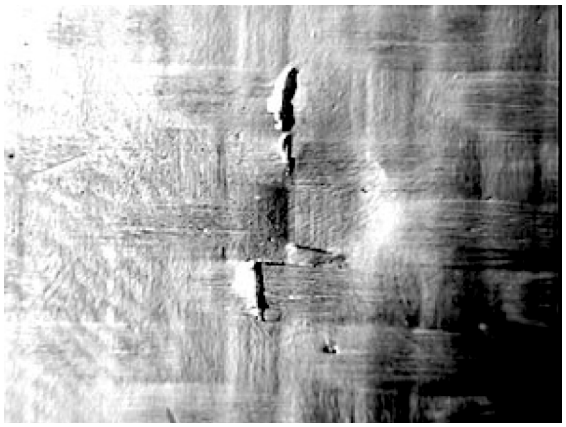

Front, Specimen 5, 1.26 ft-lb

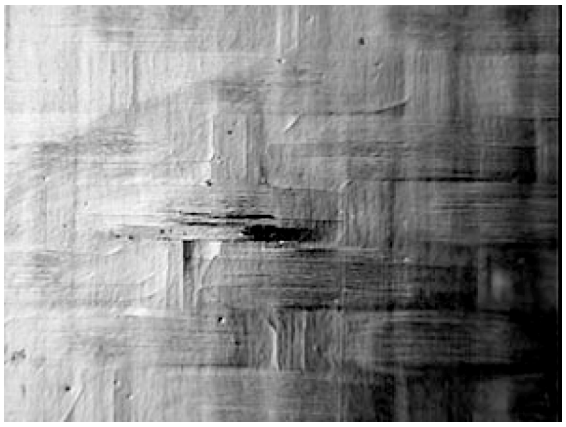

Back, Specimen 5, 1.26 ft-lb

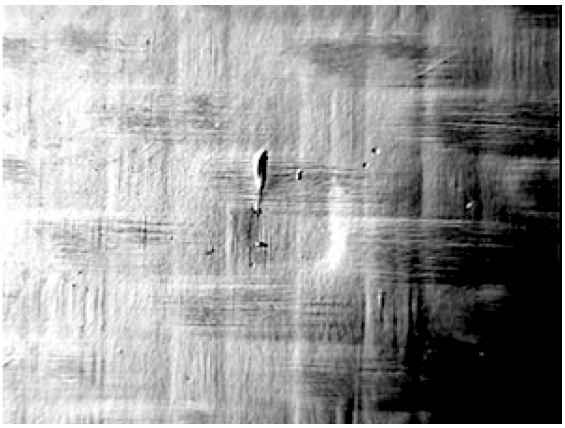

Front, Specimen 6, 0.84 ft-lb

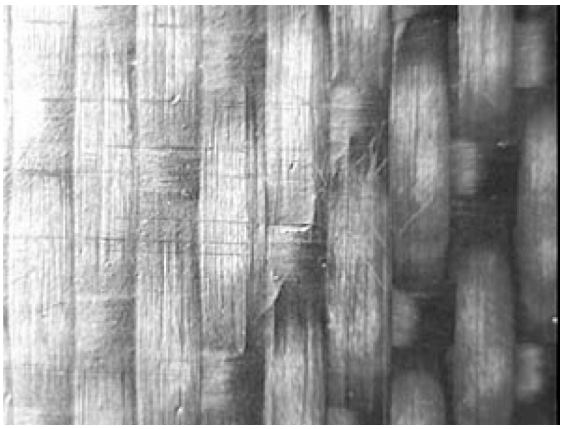

Back, Specimen 6, 0.84 ft-lb

Figure 55. Surface views of impacted HLU specimens (continued).

4.6.2.2 Leak Check Testing of Hand Layup Specimens. Figure 56 shows photographs of the specimens when subjected to a pressure of 10 psi on one side and a bubble-type leak detection solution placed on the other. Results from all specimens are included since these results did not show the duplication that was seen in the visual results. The impact energy level is included below each image.

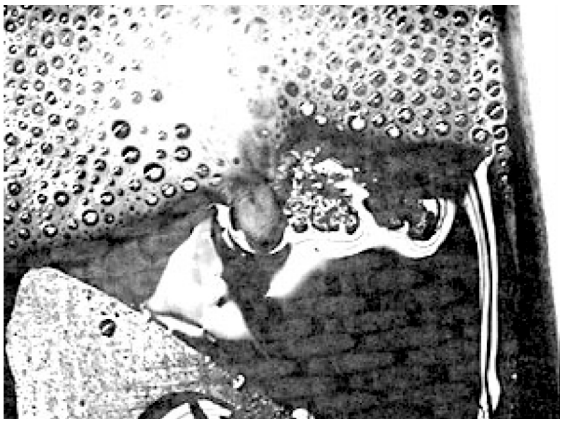

Specimen 2A, 2.51 ft-lb

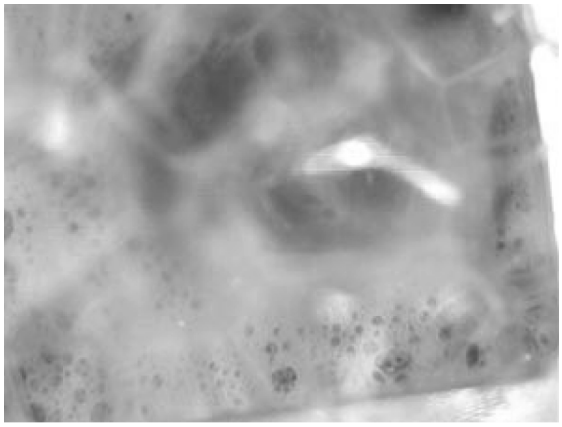

Specimen 2B, 2.51 ft-lb

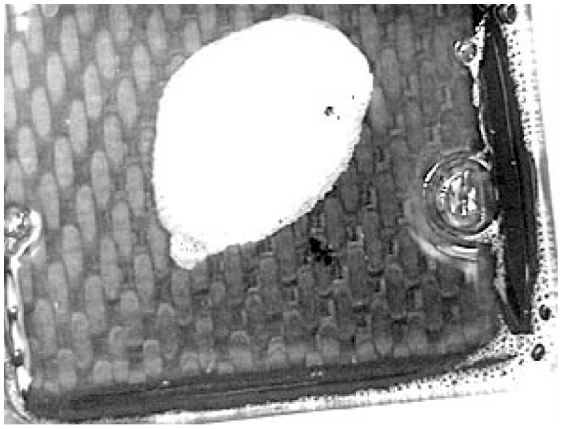

Specimen 3A, 2.09 ft-lb

Specimen 3B, 2.09 ft-lb

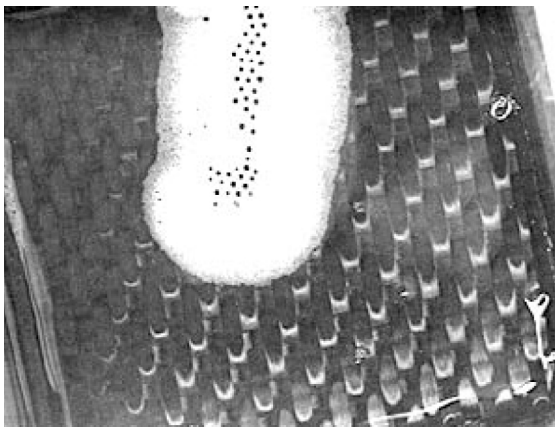

Specimen 4A, 1.67 ft-lb

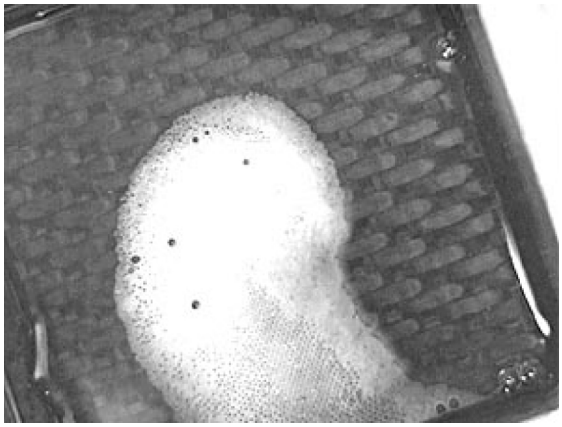

Specimen 4B, 1.67 ft-lb

Figure 56. Leak check images of HLU specimens.

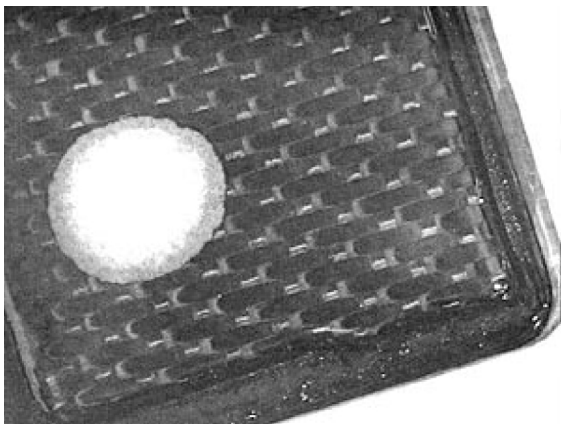

Specimen 5A, 1.26 ft-lb

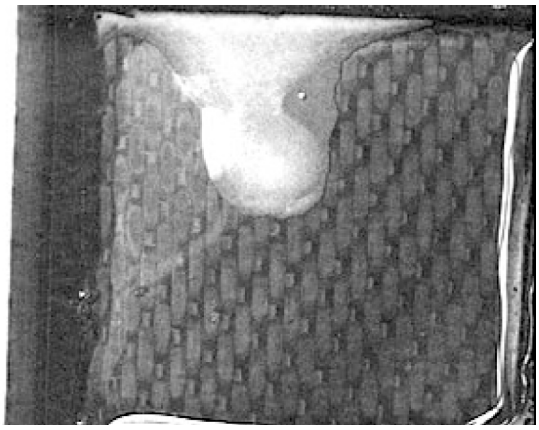

Specimen 5B, 1.26 ft-lb

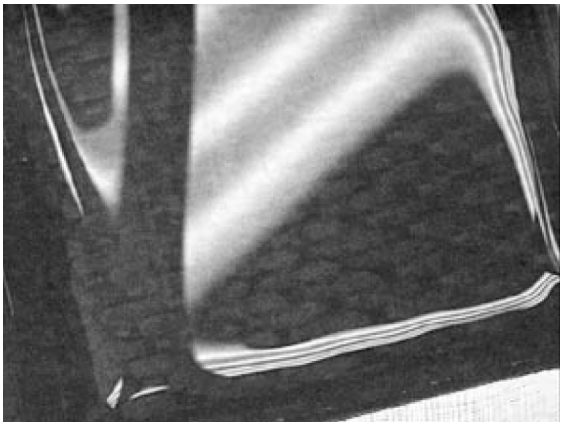

Specimen 6A, 0.84 ft-lb

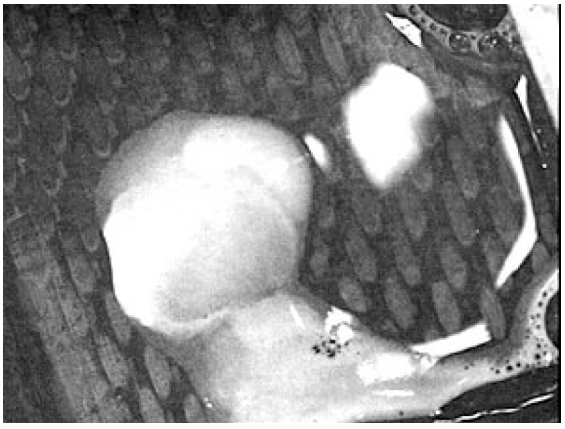

Specimen 6B, 0.84 ft-lb

Figure 56. Leak check images of HLU specimens (continued).

All samples, with the exception of 6A, showed leakage. The larger the bubbles are in the pictures, the higher the leak rate. Specimen 2B was difficult to photograph due to the extremely large bubbles that were forming. Specimen 2A can be seen to rapidly expel the leak detect solution and form relatively large bubbles. As the impact damage becomes less severe, the bubbles become smaller. In fact, in specimens 5A and 6B, the leak rate is such that the leak detection fluid forms a fine "foam" that emanates from the impacted area.

4.6.2.3 Permeability Testing of Hand Layup Specimens. Figures 57–63 show plots of flow rate versus pressure for the samples tested. Specimen 6A showed no permeability (as would be expected from fig. 56) and specimens 2A and 2B had such high flow rates that measurements could not be taken. A polynomial curve fit to the data is given in each figure.

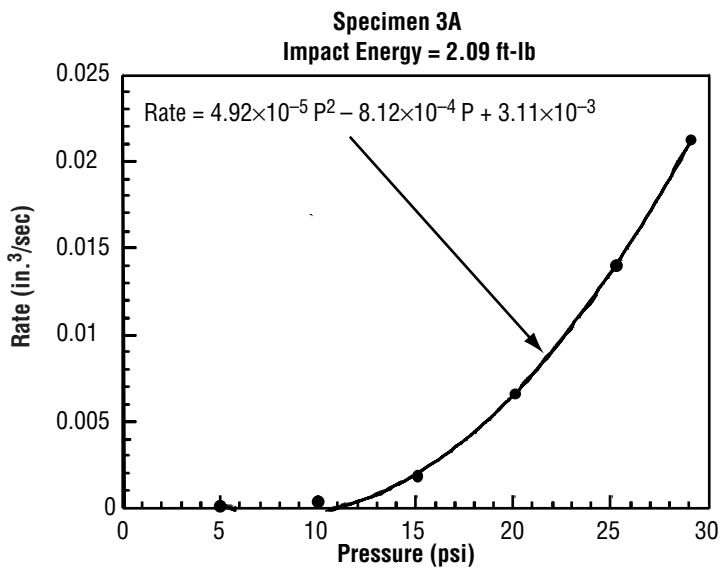

Figure 57. Flow rate (permeability) versus applied pressure for specimen 3A.

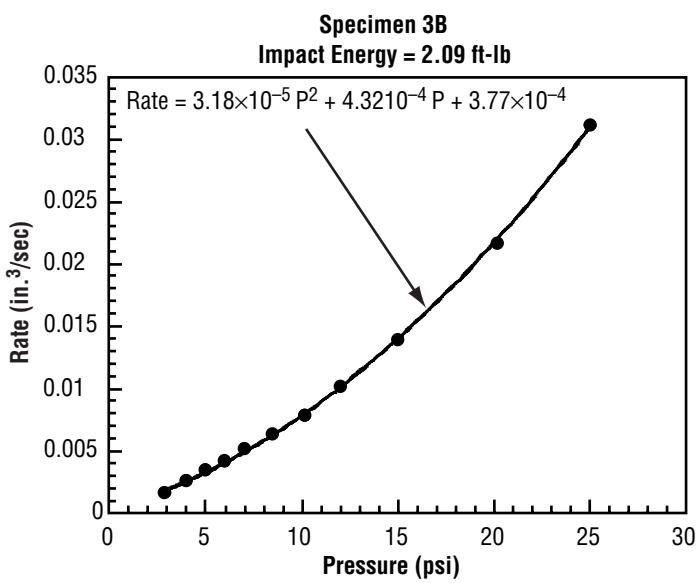

Figure 58. Flow rate (permeability) versus applied pressure for specimen 3B.

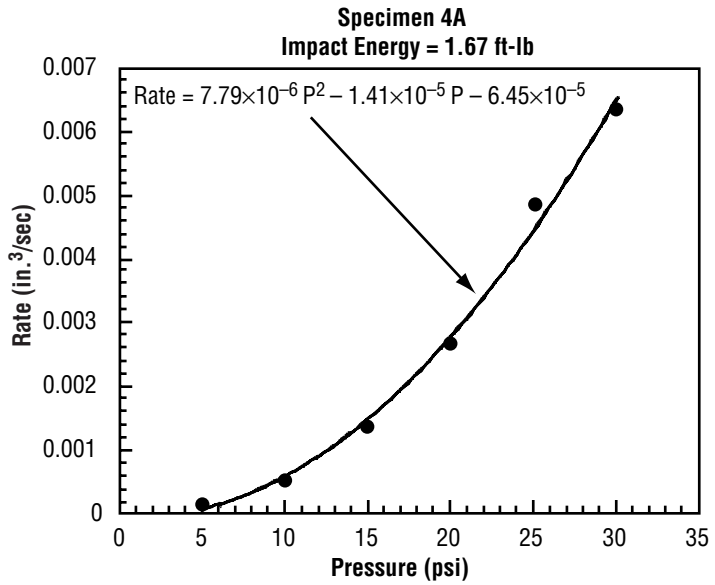

Figure 59. Flow rate (permeability) versus applied pressure for specimen 4A.

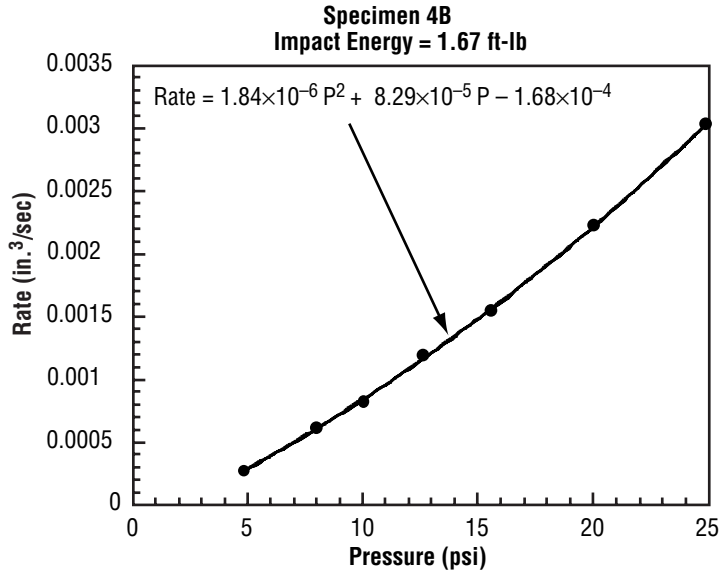

Figure 60. Flow rate (permeability) versus applied pressure for specimen 4B.

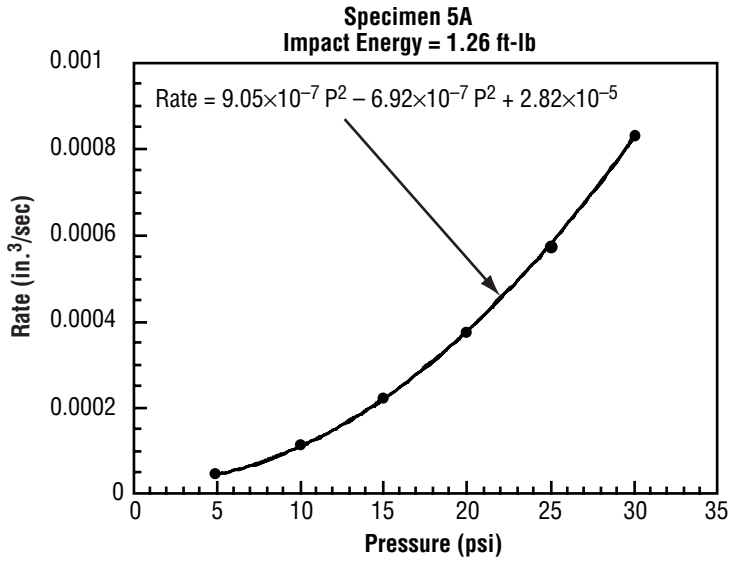

Figure 61. Flow rate (permeability) versus applied pressure for specimen 5A.

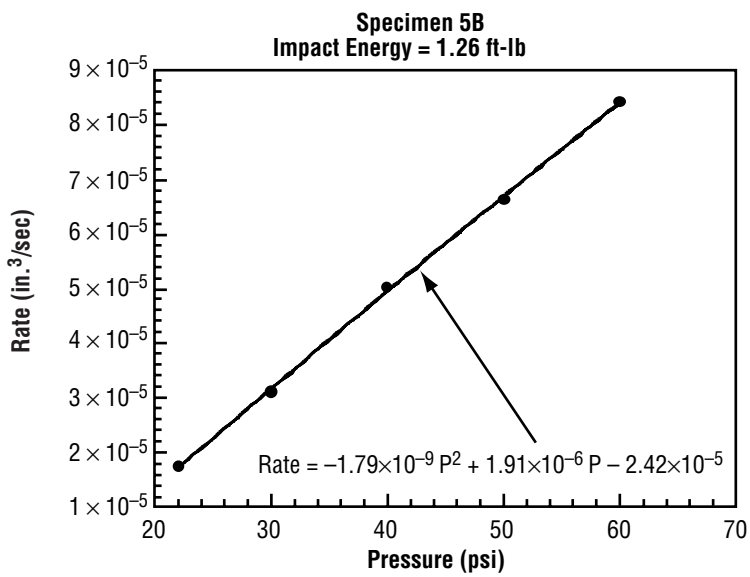

Figure 62. Flow rate (permeability) versus applied pressure for specimen 5B.

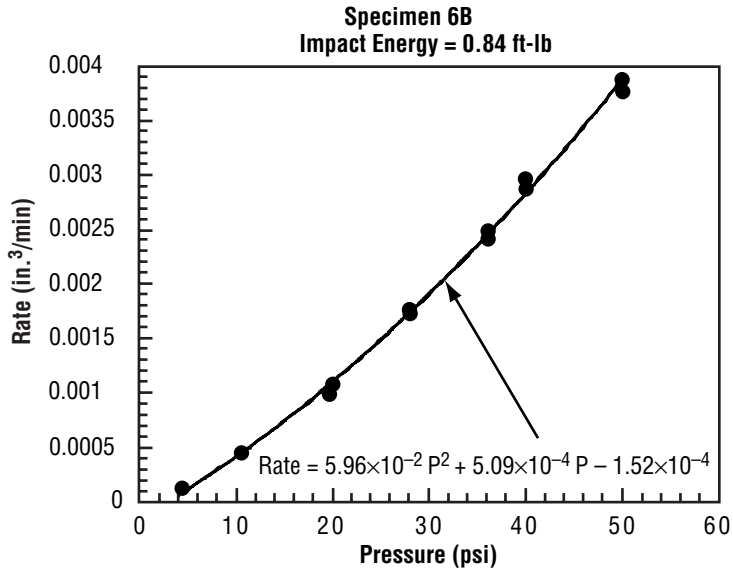

Figure 63. Flow rate (permeability) versus applied pressure for specimen 6B.

In general, the larger the impact energy, the higher the flow rate for a given applied pressure, which is expected. A noticeable exception is specimen 5B, which showed a very low flow rate, even though it was hit harder than specimen 6B. The amount of nonlinearity in flow rate versus applied pressure also varied between samples; however, most of the nonlinearity is observed at the lower pressures, and as the applied pressure increased, the linearity of the flow rate versus pressure increased.

4.6.2.4 Impact Testing of Electron Beam Specimens. Ten specimens were impacted, two at each of the five energy levels. The resulting surface damage is presented in figure 64. Duplicates are not presented. Specimen 1 (impact energy of 0.84 ft-lb) is not shown since no visible damage was present. In addition, the front of specimen 2 is not shown for the same reason. Damage is relatively light compared to comparable specimens made from the HLU technique and presented in figure 55. Less plastic deformation is seen in the electron beam-cured specimens. However, from the cross-sectional results given in figure 51, it can be seen that despite little surface damage, significant internal damage can be present in the impacted electron beam-cured specimens.

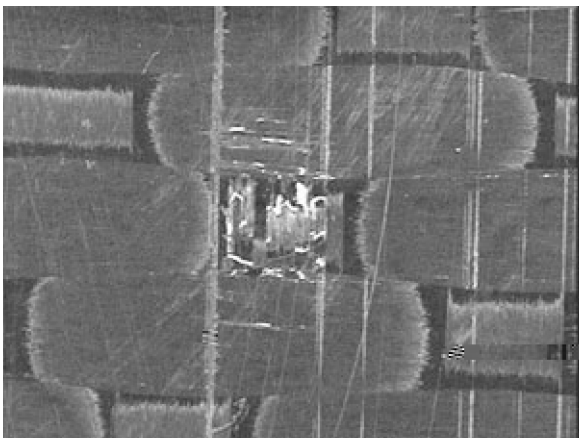

Back, Specimen 2, 1.26 ft-lb

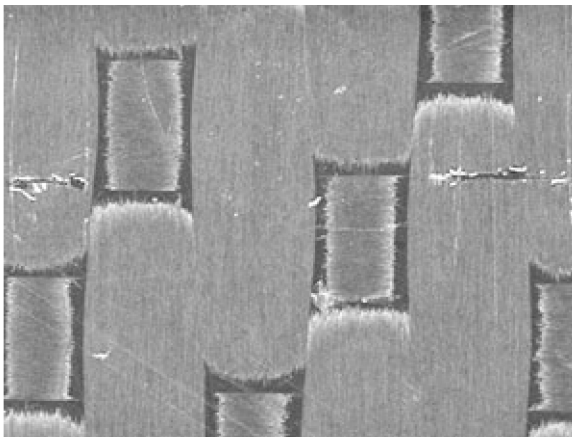

Front, Specimen 3, 1.67 ft-lb

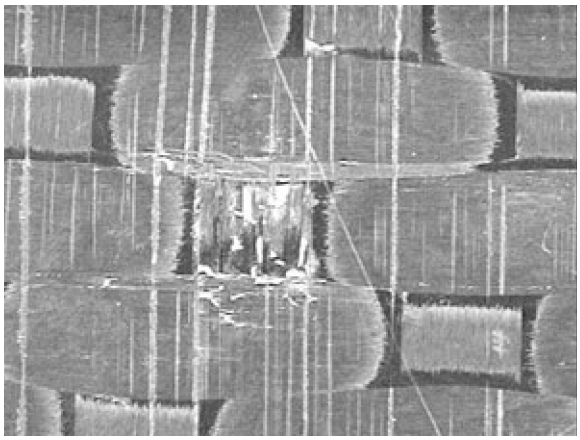

Back, Specimen 3, 1.67 ft-lb

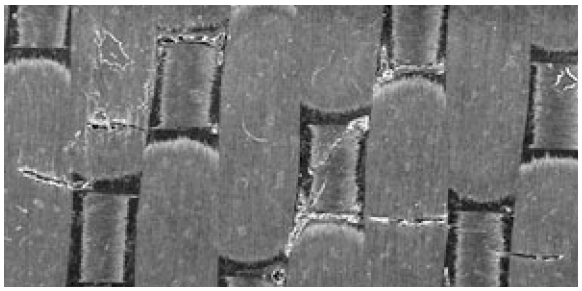

Front, Specimen 4, 2.09 ft-lb

Back, Specimen 4, 2.09 ft-lb

Figure 64. Surface views of electron beam-impacted specimens.

4.6.2.5 Leak Check Testing of Electron Beam Specimens. As the impacted electron beam specimens were being checked for visual leakage after impact, it was noted that most of the specimens were demonstrating gross leakage across the specimen, away from the impact site. A panel that had not been impacted was tested and it too showed gross areas of leakage. Since there was so much permeability of the specimen before impact, permeation after impact testing was not performed for these specimens. Figure 65 shows examples of this gross permeability on the electron beam-cured laminates.

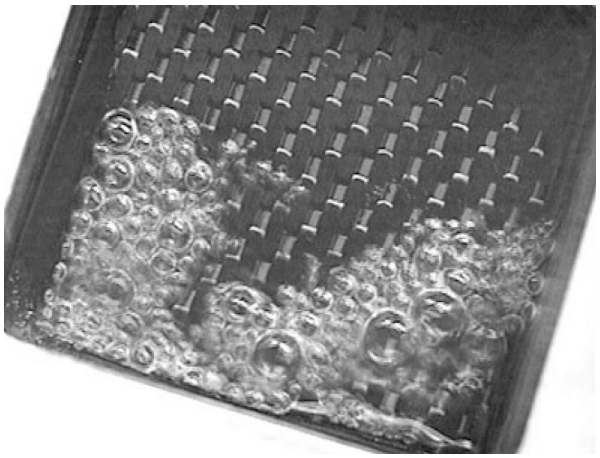

Specimen 1 showing gross leakage on one side of the specimen.

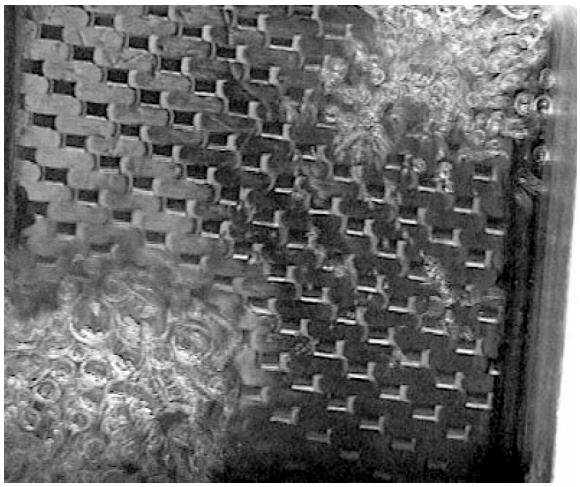

Specimen 6 showing leakage across certain areas of the laminate.

Figure 65. Examples of large areas of leakage on electron beam-cured laminates.

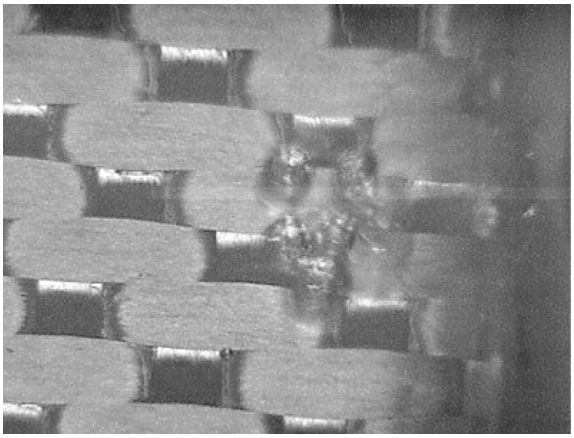

Close-up view of above specimen showing leakage at stitch.

Figure 65. Examples of large areas of leakage on electron beam-cured laminates (continued).

4.6.3 Conclusions

For permeability after impact testing, the residual flow rate usually has a nonlinear dependence on the applied pressure, increasing more rapidly as a higher pressure is applied. Thus, the permeability cannot be stated as a constant per unit of applied pressure.

The HLU four-ply laminates tested in this study showed leakage after impact, even when visible damage could only be detected with magnifying techniques. The qualitative measurement of leakage with the bubble-type leak detector solution corresponded with the qualitative permeability measurements.

The electron beam-cured laminates demonstrated gross areas of leakage/permeability across the laminate that seemed to be clustered in areas. About one-half of the electron beam specimens demonstrated this type of gross leakage.

5. ANALYSIS

A limited series of analysis was performed to compare to the actual data gathered while testing the feedlines. The model was built using PATRAN 8.5, then translated to ANSYS 5.5 for analysis. Detailed information can be obtained in the MSFC structural mechanics team report, "Stress Analysis of Marshall Space Flight Center LH_2 Composite Test Article Number 1, Drawing Number 96M00001" dated June 19, 2001, and labeled as report number ED22–01–100. For briefness, only the highlights will be presented in this TP.

Table 3 shows the predicted and actual value of the 17 strain gauges (in the hoop direction) shown in figure 17 for feedline HLU #2. The tube was assumed fixed-fixed, and the internal pressure was 150 psi.

Table 3. Predicted and actual hoop strain data for feedline HLU #2.

Gauge No.	Predicted (microstrain)	Actual (microstrain)	% Difference
1	592	424	–28.4
2	520	463	–10.9
3	520	472	–9.21
4	1444	Bad gauge	–
5	1324	2104	58.9
6	–	Bad gauge	–
7	1313	Bad gauge	–
8	1426	1413	–0.087
9	1064	404	–62.1
10	1124	407	–63.8
11	1287	2271	76.5
12	597	491	–17.8
13	576	423	–26.5
14	457	Bad gauge	–
15	1025	968	–5.5
16	993	885	–10.9
17	1028	2417	135.3

Table 4 shows the predicted and actual value of the 17 strain gauges (in the hoop direction) shown in figure 17 for feedline HLU #7. The tube was assumed fixed-fixed, and the internal pressure was 150 psi.

Table 4. Predicted and actual hoop strain data for feedline HLU #7.

Gauge No.	Predicted (microstrain)	Actual (microstrain)	% Difference
1	–	Bad gauge	–
2	–	Bad gauge	–
3	520	732	40.7
4	1444	3123	116.3
5	1324	1336	0.92
6	–	Bad gauge	–
7	1313	2200	67.6
8	1426	1651	15.8
9	1064	2330	119.0
10	1124	2112	87.9
11	1287	1881	46.2
12	597	701	17.4
13	576	803	39.0
14	457	527	15.2
15	–	Bad gauge	_
16	993	1443	45.3
17	–	Bad gauge	–

From these data, it can be seen that prediction of the elastic response of the feedline is not easy. In fact, the data from the two tests differ significantly, although all test conditions were held constant. This is most probably due to the method in which the tubes were made. To get a five-harness weave to lie down across an elbow shape with the fibers running in a particular direction is a daunting task to say the least. In addition, there are ply drops and seams that are not accounted for in the model. In fact, many of the measured values on a given gauge on the two feedlines tested actually bracket the predicted value, thus no determination of the validity of the model can be made with such large variations in the actual test data.

6. DISCUSSION AND CONCLUSIONS

The difficulty in developing an all-composite cryogenic feedline without a liner present becomes obvious in this study. The majority of the full-scale test articles that were manufactured either leaked before any testing began or leaked after just one cycle of LN_2. The only test articles that survived the entire cryogenic cycling and pressurization were two that were manufactured by the HLU and autoclave cure procedure. The feedlines that were made by SARTM sustained microcracking across their entire acreage after one cycle of LN_2. These microcracks caused gross permeation and the testing was stopped. The feedlines manufactured by TTL seemed to suffer from a lack of consolidation. Leak paths around the flange buildup area developed on all four test articles manufactured. The radius of the flanges themselves showed severe leak paths to the point where maintaining a pressure in the feedline was difficult.

Unfortunately, full-scale test articles manufactured by electron beam curing never came to fruition during this study; however, the material was evaluated for damage tolerance testing. The results showed that this material is not as tough as the epoxy system used for the HLU processing.

REFERENCES

1. Access-to-Space Summary, Office of Space Systems Development, NASA Headquarters, 1994.

2. Nettles, A.T.: "Impact Damage Resistance of Carbon/Epoxy Tubes for the DC–XA Liquid Hydrogen Feedline," *NASA TP–3583*, Marshall Space Flight Center, AL, September 1995.

3. Randazzo, S.: "Fuel Resistant Coatings for Metal and Composite Fuel Tanks," AGARD, Fuel Tank Technology, p. 20, November 1989.

4. Murry, C.F.; Newhouse, N.L.; Schimenti, J.D.; et al.: "Development of Composite Pressure Vessels With Nonmetallic Liners," AIAA, SAE, ASME, and ASEE, 28th Joint Propulsion Conference and Exhibit, Nashville, TN, July 1992.

5. Weems, D.B.; and Fay, R.E.: "A Moisture Barrier for Composite Sandwich Structure," Proceedings, American Helicopter Society National Technical Specialists' Meeting on Rotorcraft Structures, Williamsburg, VA, October 1995.

6. Stokes, E.H.: "Permeability of Rayon Based Polymer Composites," Proceedings, American Society of Mechanical Engineers, Symposium on Computational Mechanics of Porous Materials, Tucson, AZ, 1992.

7. Lance, D.G.; and Nettles, A.T.: "Low Velocity Instrumented Impact Testing of Four New Damage Tolerant Carbon/Epoxy Composite Systems," *NASA TP–3029*, Marshall Space Flight Center, AL, July 1990.

8. Brydges, W.T.; Gulati, S.T.; and Baum, G.: "Permeability of Glass Ribbon-Reinforced Composites," *Journal of Materials Science*, Vol. 10, pp. 2044–2049, December 1975.

9. Nettles, A.T.: "Permeability Testing of Impacted Composite Laminates for Use on Reusable Launch Vehicles," *NASA/TM—2001–210799*, Marshall Space Flight Center, AL, February 2001.

REPORT DOCUMENTATION PAGE

Form Approved
OMB No. 0704-0188

Public reporting burden for this collection of information is estimated to average 1 hour per response, including the time for reviewing instructions, searching existing data sources, gathering and maintaining the data needed, and completing and reviewing the collection of information. Send comments regarding this burden estimate or any other aspect of this collection of information, including suggestions for reducing this burden, to Washington Headquarters Services, Directorate for Information Operation and Reports, 1215 Jefferson Davis Highway, Suite 1204, Arlington, VA 22202-4302, and to the Office of Management and Budget, Paperwork Reduction Project (0704-0188), Washington, DC 20503

1. AGENCY USE ONLY *(Leave Blank)*	2. REPORT DATE	3. REPORT TYPE AND DATES COVERED
	October 2001	Technical Publication

4. TITLE AND SUBTITLE

Polymer Matrix Composite Lines and Ducts
(National Research Announcement 8–21 Final Report)

5. FUNDING NUMBERS

NRA 8–21 TA 7.5

6. AUTHORS

A.T. Nettles

7. PERFORMING ORGANIZATION NAMES(S) AND ADDRESS(ES)

George C. Marshall Space Flight Center
Marshall Space Flight Center, AL 35812

8. PERFORMING ORGANIZATION REPORT NUMBER

M–1029

9. SPONSORING/MONITORING AGENCY NAME(S) AND ADDRESS(ES)

National Aeronautics and Space Administration
Washington, DC 20546–0001

10. SPONSORING/MONITORING AGENCY REPORT NUMBER

NASA/TP—2001–211302

11. SUPPLEMENTARY NOTES

Prepared by the Materials Manufacturing and Processes Department, Engineering Directorate

12a. DISTRIBUTION/AVAILABILITY STATEMENT

Unclassified-Unlimited
Subject Category 24
Standard Distribution

12b. DISTRIBUTION CODE

13. ABSTRACT *(Maximum 200 words)*

Since composite laminates are beginning to be identified for use in reusable launch vehicle propulsion systems, a task was undertaken to assess the feasibility of making cryogenic feedlines with integral flanges from polymer matrix composite materials. An additional level of complexity was added by having the feedlines be elbow shaped. Four materials, each with a unique manufacturing method, were chosen for this program. Feedlines were to be made by hand layup (HLU) with standard autoclave cure, HLU with electron beam cure, solvent-assisted resin transfer molding (SARTM), and thermoplastic tape laying (TTL). A test matrix of fill and drain cycles with both liquid nitrogen and liquid helium, along with a heat up to 250 °F, was planned for each of the feedlines. A pressurization to failure was performed on any feedlines that passed the cryogenic cycling testing. A damage tolerance subtask was also undertaken in this study. The effects of foreign object impact to the materials used was assessed by cross-sectional examination and by permeability after impact testing. At the end of the program, the manufacture of the electron beam-cured feedlines never came to fruition. All of the TTL feedlines leaked heavily before any cryogenic testing, all of the SARTM feedlines leaked heavily after one cryogenic cycle. Thus, only the HLU with autoclave cure feedlines underwent the complete test matrix. They passed the cyclic testing and were pressurized to failure.

14. SUBJECT TERMS

composite materials, feedlines, impact, permeability

15. NUMBER OF PAGES

80

16. PRICE CODE

17. SECURITY CLASSIFICATION OF REPORT	18. SECURITY CLASSIFICATION OF THIS PAGE	19. SECURITY CLASSIFICATION OF ABSTRACT	20. LIMITATION OF ABSTRACT
Unclassified	Unclassified	Unclassified	Unlimited